Lithos 304–307 (2018) 230–244

Contents lists available at ScienceDirect

Lithos

journal homepage: www.elsevier.com/locate/lithos

# Mantle contribution and tectonic transition in the Aqishan-Yamansu Belt, Eastern Tianshan, NW China: Insights from geochronology and geochemistry of Early Carboniferous to Early Permian felsic intrusions

Long Du [a,b], Xiaoping Long [c,*], Chao Yuan [a], Yunying Zhang [a], Zongying Huang [a], Xinyu Wang [a], Yueheng Yang [d]

[a] State Key Laboratory of Isotope Geochemistry, Guangzhou Institute of Geochemistry, Chinese Academy of Sciences, Guangzhou 510640, China
[b] University of Chinese Academy of Sciences, Beijing 10069, China
[c] State Key Laboratory of Continental Dynamics, Department of Geology, Northwest University, Xi'an 710069, China
[d] State Key Laboratory of Lithospheric Evolution, Institute of Geology and Geophysics, Chinese Academy of Sciences, Beijing 100029, China

ARTICLE INFO

*Article history:*
Received 31 August 2017
Accepted 3 February 2018
Available online 14 February 2018

*Keywords:*
Eastern Tianshan
Aqishan-Yamansu belt
Felsic plutons
Crustal evolution
Tectonic transition

ABSTRACT

Late Paleozoic is a key period for the accretion and collision of the southern Central Asian Orogenic Belt (CAOB). Here, we present new zircon U–Pb ages, whole-rock geochemistry and Sr–Nd isotopic compositions for four Late Paleozoic felsic plutons in Eastern Tianshan (or Tienshan in some literatures) in order to constrain the tectonic evolution of the southern CAOB. The granodioritic pluton and its dioritic enclaves were synchronously formed in the Early Carboniferous (336 ± 3 Ma and 335 ± 2 Ma, respectively). These rocks are depleted in Nb, Ta and Ti, and enriched in Rb, Ba, Th and U related to the primitive mantle, which show typical features of arc rocks. They both have similar Sr–Nd isotopic ratios to those granitic rocks from the eastern Central Tianshan Block and have the latest Mesoproterozoic two stage Nd model ages ($T^2_{DM}$) (1111–1195 Ma for the granodioritic pluton and 1104–1108 Ma for the enclaves, respectively), indicating that their source magmas may have been derived from the Mesoproterozoic crust. The albitophyric pluton was also emplaced in the Early Carboniferous (333 ± 3 Ma). Rocks of this pluton have similar $\varepsilon_{Nd}(t)$ values (−0.69 to −0.37) and $T^2_{DM}$ ages (1135–1161 Ma) to those of the granodioritic rocks, suggest similar crustal source for both types of rocks. In contrast, the K-feldspar granitic and monzonitic plutons were emplaced in the Early Permian (292 ± 3 Ma and 281 ± 2 Ma, respectively). Samples of the K-feldspar granitic pluton have high $K_2O + Na_2O$, FeO/MgO, Ga/Al, HFSE (e.g., Zr and Hf) and low CaO, Sr and Ba, exhibiting characteristics of $A_2$-type granites, which probably emplaced in a post-collisional extension environment. They have higher $\varepsilon_{Nd}(t)$ values (+2.77 to +3.27) and more juvenile $T^2_{DM}$ ages (799–841 Ma) than the Early Carboniferous plutons, suggesting that they were derived from relatively younger crustal sources. The monzonitic granites are metaluminous to weakly peraluminous with A/CNK ranging from 0.93 to 1.05, and have very low $P_2O_5$, indicating characteristics of I-type granites. They also have positive $\varepsilon_{Nd}(t)$ values (+2.22 to +2.34) and juvenile $T^2_{DM}$ ages (868–878 Ma), suggesting this pluton was also produced by partial melting of relatively young crustal source. Based on an isotopic mixing simulation, significant mantle contributions were added to the magma source of both the Early Carboniferous and the Early Permian felsic rocks. The mantle contribution changes from ~60% in the Early Carboniferous to ~75% in the Early Permian. The remarkably increasing of mantle materials in the magma source of the felsic rocks in the Aqishan-Yamansu belt was most likely induced by the tectonic transition from an Early Carboniferous continental arc to an Early Permian post-collisional extension environment.



## 1. Introduction

The Central Asian Orogenic Belt (CAOB), also known as the Altaid orogenic collage (Sengör et al., 1993; Sengör and Natalin, 1996; Yakubchuk, 2004), located between the European and Siberian cratons to the north, and the Tarim and North China cratons to the south (Fig. 1a), is one of the largest accretionary orogenic belts in the world (Jahn et al., 2004; Sengör et al., 1993; Xiao et al., 2008, 2013; Yakubchuk, 2004). In contrast to the classic collisional orogenic belts, such as the Alpine, Himalayan, Hercynian and Caledonian orogens, which were formed by amalgamation of two continental blocks (Jahn et al., 2000a, 2000b; Yuan et al., 2007), the CAOB was formed by the long-lived accretion of island arcs, accretionary prisms, ophiolites and microcontinents (Jahn et al., 2000a, 2000b; Kröner et al., 2007; Sengör et al., 1993; Sengör and Natalin, 1996; Windley et al., 1990, 2007). The

* Corresponding author.
*E-mail address:* longxp@nwu.edu.cn (X. Long).

https://doi.org/10.1016/j.lithos.2018.02.010
0024-4937/

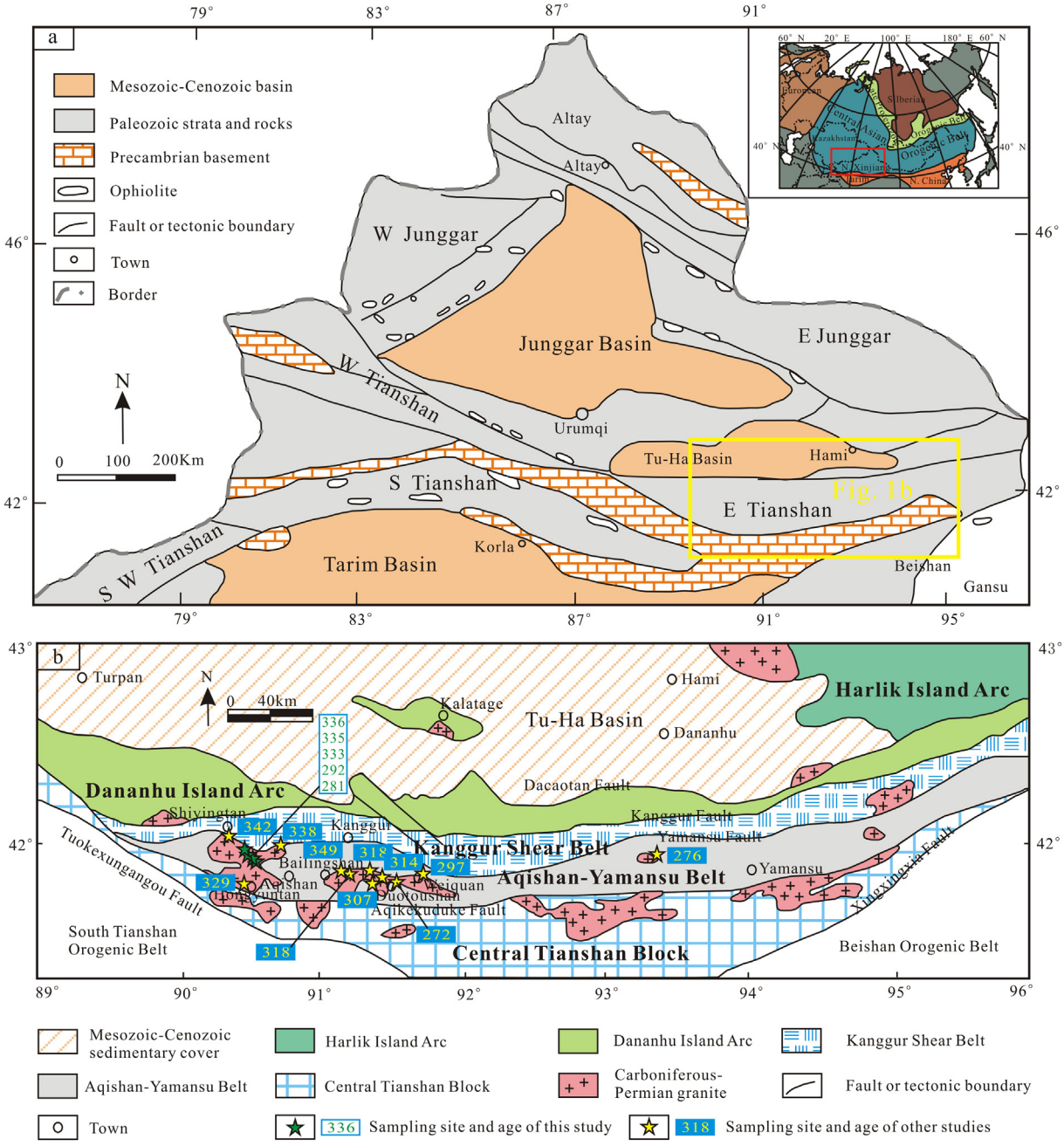


**Fig. 1.** (a) The relationship of the study area with the CAOB (after Gao et al., 2011 and Chen et al., 2012). (b) Geological map of Eastern Tianshan (after W.F. Zhang et al., 2016). Age data (Ma) are from Wang et al. (2005), Wu et al. (2006), Zhou et al. (2010) and Zhang et al. (2013), W.F. Zhang et al. (2016).

significant feature of the CAOB is the vast expanse of granitic and volcanic rocks that are characterized by positive $\varepsilon_{Nd}(t)$ and young $T_{DM}$ model ages (Jahn et al., 2000c, 2004; Tang et al., 2017; Wu et al., 2002). It is believed that at least half of its crustal growth was due to the addition of juvenile material, by both lateral and vertical accretion during the Neoproterozoic and Paleozoic (Jahn et al., 2004; Sengör et al., 1993; Tang et al., 2017; Yuan et al., 2007). As an important component of the CAOB, the Chinese Tianshan Orogenic Belt is a result of continental collision between the Tarim Craton and the Junggar Block (Fig. 1a; Jahn et al., 2004; Xiao et al., 2004, 2013; W.F. Zhang et al., 2016). In this orogenic belt, most of the juvenile crust was considered to be restricted to relatively short time periods at about 300 ± 10 Ma (Tang et al., 2017). In the eastern part of the orogenic belt (namely Eastern Tianshan or the Eastern Tianshan Orogenic Belt), voluminous Carboniferous to Permian volcanic rocks and granitoids are extensively exposed and recorded the whole or part of the tectonic history from subduction, back-arc rifting to continental accretion, and then to post-orogenic extension (Luo et al., 2016; Xiao et al., 2004, 2008, 2013; W.F. Zhang et al., 2016). Although several geochemical studies in the Eastern Tianshan have focussed on petrogenesis of the Paleozoic magmatic rocks, the regional tectonic evolution and the proportion of juvenile material in the crustal rocks are poorly constrained (Hou et al., 2014; Luo et al., 2016; W.F. Zhang et al., 2016).

Granitoid rocks, as results of the evolution of continental crust (Bonin et al., 1998; Frost et al., 2001; Ma et al., 2015; Wu et al., 2007), can provide an important probe for determining the chemical compositions of magma source and the petrogenesis (Patiño Douce, 1999; Rapp and Watson, 1995), and thus are significant to understand the processes of crustal growth (Jahn et al., 2000a, 2000b; Jahn et al., 2004). In Eastern Tianshan, Late Paleozoic granitic intrusions are extensively exposed in

Aqishan-Yamansu belt (Fig. 1b), but few of them have been investigated (Zhou et al., 2010). In order to unravel the proportion of juvenile materials invovled in the crustal growth and the Late Paleozoic geodynamic evolution of Eastern Tianshan, we present new zircon U–Pb ages, whole-rock geochemical and Sr–Nd isotopic data for four felsic intrusions in the Aqishan-Yamansu belt and also provide a synthesis of over 130 Sr–Nd isotopic data and zircon ages in the adjacent areas.

## 2. Geological background

The Chinese Tianshan Orogenic Belt is a complex collage of island arc assemblages, remnants of oceanic crust, oceanic plateaus, ophiolites and microcontinental fragments (Charvet et al., 2007, 2011; SengÖr and Natalin, 1996; Windley et al., 1990, 2007; Xiao et al., 2004). It can be geographically divided into western and eastern segments roughly along the Urumqi-Korla road, which experienced remarkably different evolution during the Paleozoic time (Gao et al., 2009; Windley et al., 1990; Xiao et al., 2004). This study focuses mainly on Eastern Tianshan and it is further divided into the Dananhu island arc belt, the Kangguer shear belt, the Aqishan-Yamansu belt and the Central Tianshan Block that are separated by Kangguer, Yamansu and Aqikekuduke faults, respectively (Fig. 1b; Xiao et al., 2004, 2013; Charvet et al., 2007, 2011).

The Dananhu belt is mainly composed of Ordovician to Devonian-Carboniferous volcanic and pyroclastic rocks and accretionary complexes composed of turbidite, basalt, chert, and ultramafic rock (Qin et al., 2002; Xiao et al., 2004). Based on the combination of regional geology and isotopic age, the Ordovician-Carboniferous tholeiitic basalts, calc-alkaline andesites and granitoids have been interpreted to be part of original island arc (Xiao et al., 2004, 2013). Recently, the report of 435–438 Ma high-Mg andesites and 437–447 Ma arc-type granitic plutons in the Kalatag area (Du et al., 2018; Li et al., 2016; Long et al., 2016) have provided reliable evidence of an Early Paleozoic magmatic arc in the Dananhu belt. The Dananhu belt is characterized by the presence of Early Paleozoic sediments and the absence of passive continental margin sediments (Du et al., 2018; Li et al., 2016; Long et al., 2016), indicating that the formation of the Dananhu arc was prior to, or begun at, the Late Ordovician, due to north-dipping subduction of the Kangguer oceanic lithosphere (Du et al., 2018).

In fault contact with the Dananhu arc to the north, the Kangguer belt is mainly occupied by Carboniferous sedimentary and volcanic rocks, including conglomerate, sandstone, siltstone, bioclastic limestone, basaltic and andesitic tuff (BGMRXUAR, 1993; B. Wang et al., 2014; Xiao et al., 2013). Devonian rocks only occur in the north of this region and consist of basalt and andesite with minor rhyolite, dacite, volcanic breccia, tuff and clastic rocks. Lower Permian volcanic rocks recognized locally in the Kangguertag area unconformably overlie the Carboniferous sequence and are in turn overlain by middle and upper Permian arkose, which is interlayered with conglomerate (BGMRXUAR, 1993). Ophiolites with late Cambrian age (494 ± 10 Ma) (Li et al., 2008) occur along the Kangguer fault representing remnants of the Kangguer ocean plate. Recently, SHRIMP zircon U–Pb dating for the Dongdagou lithic sandstone from the Kangguertage ophiolite yielded an age of 330 Ma (Liu et al., 2016). Because the lithic sandstone was structural integrated over the Kangguertage ophiolite associations (pillow basalt and siliceous rocks), this age was considered as the minimum age for the Kangguertage ophiolite.

The Aqishan-Yamansu belt, located between the Yamansu Fault in the north and the Aqikeduke Fault in the south, mainly contains two marine units: the Early Carboniferous Yamansu Formation and the Late Carboniferous Tugutublak Formation (Muhetaer et al., 2014; W.F. Zhang et al., 2016). Rocks of the Yamansu Formation are mainly exposed in the northern part of the Aqishan-Yamansu belt and have some index fossils, such as Arachnolasma, Gigantoprductus and Yuanophyllum (Zhang et al., 2012; W.F. Zhang et al., 2016), whereas rocks of the Tugutublak Formation are distributed in the southern part and have corals and fusulinids within the intercalated limestone (Zhang et al., 2012; W.F. Zhang et al., 2016). Numerous arc-related late Paleozoic granitoids have intruded the Early Carboniferous Yamansu Formation and the Late Carboniferous Tugutublak Formation (Fig. 1b; Wang et al., 2005; Wu et al., 2006; Zhou et al., 2010; Zhang et al., 2013; W.F. Zhang et al., 2016).

The Central Tianshan Block is separated from the Aqishan-Yamansu belt to the north by the Aqikeduke fault and the Tarim Craton to the south by the Tuokexun-Xingxingxia fault. It predominantly consists of Precambrian-Mesozoic magmatic and sedimentary rocks (Li et al., 2016; Xiao et al., 2004; X.R. Zhang et al., 2016). The Precambrian basement rocks were divided into the Tianhu, Kawabulag and Xingxingxia groups, most of which have undergone greenschist-to-amphibolite facies metamorphism and are unconformably overlain by or in fault contact with Paleozoic strata (Hu et al., 1998; Huang et al., 2017; X.R. Zhang et al., 2016). The basement is mainly composed of gneisses and migmatites covered by Precambrian meta-sedimentary rocks including clastic rocks, limestones and quartzites (1458–730 Ma) (Huang et al., 2015, 2017). Early Paleozoic to Early Mesozoic assemblages of ultramafic to felsic volcanic rock, granitoid, graywacke and flysch rock are exposed in the Central Tianshan Block (Ma et al., 2014, 2015; X.R. Zhang et al., 2016).

## 3. Sampling and petrography

Twenty-five fresh igneous samples from four plutons near the Aqishan Mountain (Fig. 1b) were collected for analyses in this study. The granodiorite samples are medium to coarse-grained with equigranular texture. They mainly consist of quartz (45–35%), plagioclase (40–35%), K-feldspar (10–5%), biotite (~5%) and amphibole (~5%) with minor accessory minerals (<5%) (Fig. 2a, d). The fine-grained dioritic enclaves are gabbroic to dioritic in composition with oval shapes and variable size. They have the same mineral assemblages as the granodiorite but with higher proportion of mafic minerals such as amphibole (35–20%) and biotite (10–5%) (Fig. 2a, e, f). The albitophyre samples are massive and porphyritic in texture and mainly contain albite (45–30%) and quartz (40–30%) with zircon and apatite as accessory minerals (Fig. 2g). The K-feldspar granite samples mainly consist of quartz (40–35%), K-feldspar (35–25%), plagioclase (~10%), amphibole (~10%), and biotite (~5%), with minor accessory minerals (<5%) (Fig. 2b, h). The monzonitic granite samples have more plagioclase and less K-feldspar than the K-feldspar granites, with similar contents of other minerals (Fig. 2c, i).

## 4. Analytical methods

### 4.1. Zircon U–Pb dating

Zircons were separated from fresh samples using standard density and magnetic techniques and then selected under a binocular microscope. They were polished to about half section before Cathodoluminescence (CL) imaging using a JXA-8100 Electron Probe Microanalyzer with a Mono CL3 Cathodoluminescence System at State Key Laboratory of Isotope Geochemistry, Guangzhou Institute of Geochemistry, Chinese Academy of Sciences.

In situ zircon U–Pb and trace element analyses were conducted utilizing a laser ablation inductively coupled plasma mass spectrometry system (LA-ICP-MS) at the Institute of Geology and Geophysics, Chinese Academy of Sciences. Laser ablation was accomplished using a Geolas-193 laser-ablation system equipped with a 193 nm ArFexcimer laser and the isotopes and elements were measured by an ELAN6100 DRC ICP-MS. The analyses were conducted with a spot diameter of 44 μm with a typical ablation time of approximately 30 s for 200 cycles of each measurement, an 8 Hz repetition rate, and a laser power of 100 mJ/pulse (Yang et al., 2006b). A more detailed description of the analytical technique is similar to those documented by Yuan et al. (2004). Isotopic ratios were calculated using GLITTER 4.0 (Griffin et al., 2008),

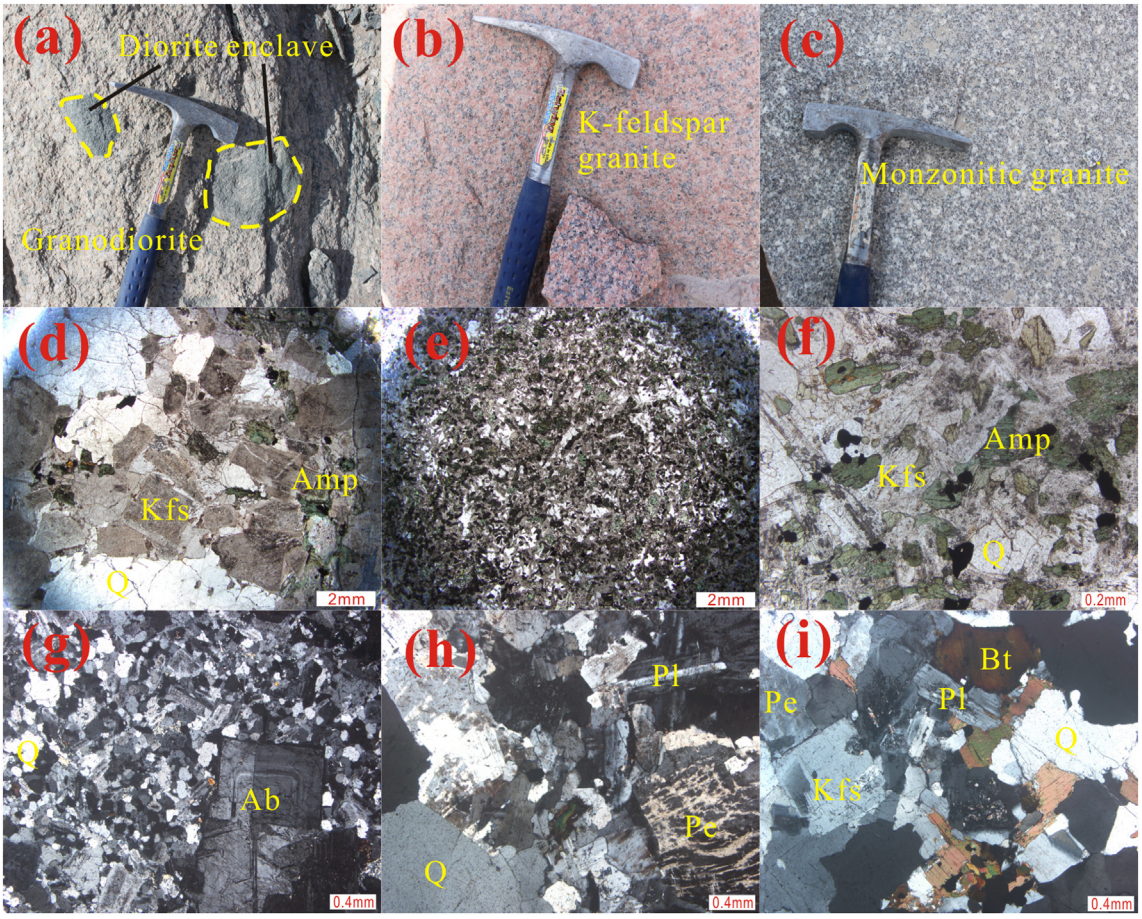


**Fig. 2.** (a), (b) and (c) Field photos of the Late Paleozoic felsic plutons in the Aqishan-Yamansu belt. (d)–(i) Textural characteristics of the Late Paleozoic rcoks as seen in thin-section under plane-polarized or cross-polarized light. (d) Granodiorite; (e) and (f) Dioritic enclave; (g) Albitophyre; (h) K-feldspar granite; (i) Monzonitic granite. Mineral abbreviations: Ab-Albite, Amp-Amphibole, Bt-Biotite, Kfs-K-feldspar, Pe-Perthite, Pl-Plagioclase and Q-Quartz.

and age calculation and plotting of Concordia diagrams was performed using Isoplot/Ex 3.0 (Ludwig, 2003).

### 4.2. Whole-rock geochemistry

Major element oxides of whole-rock samples were determined on fusion glasses with a 1:8 sample to $Li_2B_4O_7$ flux ratio, using a Rigaku ZSX100e X-ray fluorescence spectrometer (XRF) at State Key Laboratory of Isotope Geochemistry, Guangzhou Institute of Geochemistry. The accuracies of the XRF analyses are between 1% and 5%. Trace elements, including the rare earth element (REE), were analyzed by a Perkin-Elmer ELAN 6000 inductively-coupled plasma source mass spectrometer (ICP-MS) at the State Key Laboratory in Guangzhou Institute of Geochemistry. Powdered samples (50 mg) were digested in screw-top Teflon beakers with an HF + $HNO_3$ mixture for 7 days at about 100 °C in order to assure complete dissolution of the refractory minerals. An internal standard solution containing the single element Rh was used to monitor signal drift in mass response during counting. USGS standards G-2, W-2, MRG-1 and AGV-1 and Chinese national rock standards GSD-12, GSR-1, GSR-2 and GSR-3 were used to calibrate the elemental concentrations of the measured samples. The accuracies of the ICP-MS analyses for some transition elements (Cr, V, Cu amd Zn) are better than 10%, for the rest elements are generally better than 5% (Liu et al., 1996). Sample preparation techniques and other details of procedures are described as same in the references (Long et al., 2012, 2015).

Whole–rock Sr–Nd isotopic measurements were performed on a Micromass Isoprobe multi-collector ICP-MS at the Guangzhou Institute of Geochemistry, using analytical procedures described by Li et al. (2006). Sr and REE were separated using cation columns, and Nd fractions were further separated by HDEHP-coated Kef columns. The measured Sr and Nd compositions were corrected for mass fractionation to $^{86}Sr/^{88}Sr = 0.1194$ and $^{146}Nd/^{144}Nd = 0.7219$, respectively. The reported $^{87}Sr/^{86}Sr$ and $^{143}Nd/^{144}Nd$ ratios were respectively adjusted to the NBS SRM987 standard ($^{87}Sr/^{86}Sr = 0.71025$) and the Shin Etsu JNdi-1 standard ($^{143}Nd/^{144}Nd = 0.512115$).

## 5. Analytical results

### 5.1. Zircon U–Pb age

The granodiorite sample (X3SS01) as well as the dioritic enclave sample (X3SS08) has been dated. Zircons from the granodiorite sample are euhedral, prismatic crystals with length/width ratios 2 to 3, and have concentric oscillatory zoning in CL images in good agreement with igneous zircons (Fig. 3a). Three (spot 06, 18, 19) of twenty-one analyzed zircons were plotted to be away from the Concordia curve probably due to partial Pb loss and the other eighteen analyses yield a Concordia age of 336 ± 3 Ma (MSWD = 4.9) (Fig. 3a and Supplemental Table S1). Zircon grains from the dioritic enclave show similar shapes to zircon from the host granodiorite and also exhibit typical characteristics of igneous zircons with oscillatory zoning. Nineteen analyses yield a weighted mean age of 335 ± 2 Ma (MSWD = 0.92) (Fig. 3b and Supplemental Table S1), indicating that the granodioritic pluton and its dioritic enclaves were both emplaced in the Early Carboniferous.

Zircon grains from albitophyre sample (X3SS14) are generally transparent, stubby to prismatic, with concentric oscillatory zoning in CL, consistent with an igneous origin. We have analyzed twenty zircons, of which one analysis (No. 13) plots above the Concordia curve and

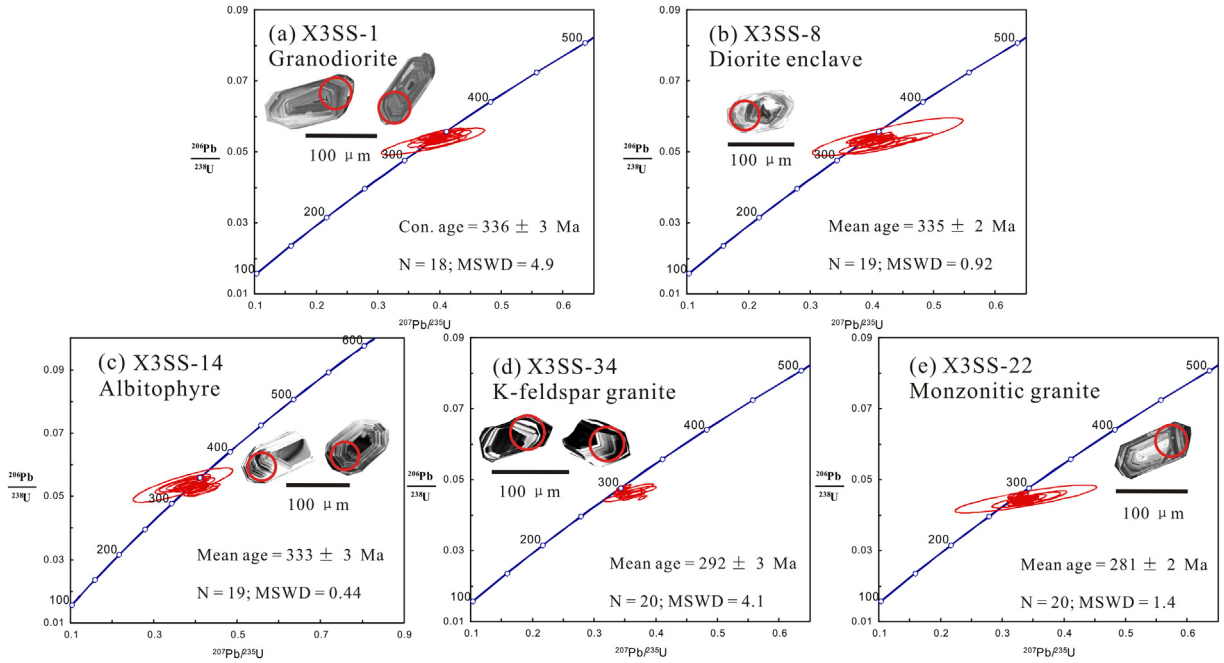


**Fig. 3.** Concordant diagrams of zircons from the Late Paleozoic rocks in the Aqishan-Yamansu Belt.

gives apparent $^{206}Pb/^{238}U$ age of 349 ± 4 Ma (Supplemental Table S1). The other nineteen zircons yield a weighted $^{206}Pb/^{238}U$ mean age of 333 ± 3 Ma (MSWD = 0.44) (Fig. 3c and Supplemental Table S1). This age is considered to be the emplacement age of the albitophyric pluton.

Zircons from the K-feldspar granite (sample X3SS34) show similar shapes to zircon from those Early Carboniferous plutons and also exhibit typical characteristics of igneous zircons with oscillatory zoning. Twenty grains were analyzed and four (spot 02, 06, 07, 11) of them plot away from the Concordia maybe attribute to partial Pb loss. Although Pb loss may cause large uncertainties in $^{207}Pb/^{206}Pb$ and $^{207}Pb/^{235}U$ ratios (Fan et al., 2012), these zircons show similar apparent $^{206}Pb/^{238}U$ ages ranging from 283 Ma to 301 Ma, which yield a weighted mean $^{206}Pb/^{238}U$ age of 292 ± 3 Ma (Fig. 3d and Supplemental Table S1). This age is interpreted as the crystallization age of the K-feldspar granitic pluton.

Zircons from the monzonitic granite (sample X3SS22) also display clear oscillatory zoning. Twenty-one zircons were analyzed. Except one grain plots away from the Concordia, the others yield a weighted mean $^{206}Pb/^{238}U$ age of 281 ± 2 Ma (MSWD = 1.4) (Fig. 3e and Supplemental Table S1), which is considered to be the emplacement age of the monzonitic granitic pluton.

### 5.2. Whole-rock geochemistry

#### 5.2.1. Granodiorite

The granodioritic samples display high $SiO_2$ (69.9–72.5 wt.%), low MgO (0.84–1.01 wt.%), $Fe_2O_3^T$ (2.72–3.31 wt.%) and $TiO_2$ (0.27–0.33 wt.%) contents (Table 1). They are characterized by moderate total alkali ($K_2O + Na_2O$ = 6.10–6.98 wt.%) and $K_2O/Na_2O$ (0.53–0.66), showing medium-K to high-K calc-alkaline characteristics (Fig. 4a, b and Table 1). These samples are weakly metaluminous to weakly peraluminous with ASI (aluminum saturation index: molecular $Al_2O_3/(Na_2O + K_2O + CaO)$) values ranging from 0.94 to 1.07 (Fig. 4c and Table 1). In the Chondrite-normalized diagram, they have uniform REE patterns and are characterized by LREE enrichment ($(La/Yb)_N$ = 5.72–6.52), with flat HREE patterns ($(Ga/Yb)_N$ = 1.04–1.10) and negative to positive Eu anomalies ($Eu/Eu^*$ = 0.71–1.03) (Fig. 5a and Table 1). These rocks have relatively high large ion lithophile element (LILE) concentrations, such as Rb (76.3–103 ppm), Ba (426–670 ppm) and Sr (149–228 ppm), but low Cr (3.41–5.92 ppm), Co (4.92–5.97 ppm) and Ni (1.52–2.28 ppm) (Table 1). In a primitive mantle normalized diagram, these samples show strong negative Nb, Ta and Ti anomalies, and display positive Rb, Ba and Pb anomalies (Fig. 5b). These rocks have a narrow range of initial $^{87}Sr/^{86}Sr$ ratios (0.7050 to 0.7052) and $\varepsilon_{Nd}(t)$ (−1.06 to −0.05) with two stage Nd model ages ($T^2_{DM}$ = 1111–1195 Ma) (Table 2).

#### 5.2.2. Dioritic enclave

Samples from the dioritic enclaves are mafic to intermediate in composition with $SiO_2$ ranging from 53.8 to 58.8 wt.% (Table 1). They have MgO (2.86–3.52 wt.%), $Fe_2O_3^T$ (8.49–9.55 wt.%) and $TiO_2$ (0.62–0.87 wt.%) contents higher, but total alkali ($K_2O + Na_2O$ = 5.09–6.45 wt.%) and $K_2O/Na_2O$ (0.37–0.41) lower than the granodiorite pluton (Table 1). The samples are metaluminous with ASI values ranging from 0.81 to 0.90 (Fig. 4c and Table 1). In the Chondrite-normalized diagram, they are characterized by less significant LREE enrichment ($(La/Yb)_N$ = 2.66–4.55), but with similar flat HREE patterns ($(Ga/Yb)_N$ = 0.92–1.14) and slightly negative Eu anomalies ($Eu/Eu^*$ = 0.64–1.03) compared with the host granodiorite samples (Fig. 5a and Table 1). These rocks also have relatively high LILE concentrations, such as Rb (62.4–76.3 ppm), Ba (308–556 ppm) and Sr (231–272 ppm), but low Cr (3.63–5.12 ppm) and Ni (3.04–4.72 ppm), slightly higher Co (19.3–20.6 ppm) (Table 1). In a primitive mantle normalized diagram, these samples also display strong negative Nb, Ta and Ti anomalies, and show positive Rb, Ba and Pb anomalies (Fig. 5b). Compared with the host granodiorite rocks, they have a similar narrow range of initial $^{87}Sr/^{86}Sr$ ratios (0.7056 to 0.7059) and slightly higher $\varepsilon_{Nd}(t)$ (−0.02 to 0.03) with similar Mesoproterozoic $T^2_{DM}$ ages (1104–1108 Ma) (Table 2).

#### 5.2.3. Albitophyre

The albitophyric samples have high $SiO_2$ (71.2–76.4 wt.%) and $Na_2O$ (5.60–7.80 wt.%), low $Fe_2O_3^T$ (0.11–0.81 wt.%) and $K_2O$ (0.17–0.61 wt.%), and thus have very high $Na_2O/K_2O$ ratios (10.6–34.6) (Table 1). They have ASI index between 0.84 and 0.93, displaying a weakly metaluminous character (Fig. 4c and Table 1). The samples are LREE-enriched ($(La/Yb)_N$ = 1.89–7.23), but show uniform flat HREE patterns ($(Ga/Yb)_N$ = 0.97–1.07) and negative Eu anomalies ($Eu/Eu^*$ = 0.60–0.76) (Fig. 5c and Table 1). These rocks have low Rb

**Table 1**
Major and trace element compositions of the Late Paleozoic felsic plutons.

| Sample | X3SS-2 | X3SS-3 | X3SS-4 | X3SS-5 | X3SS-6 | X3SS-9 | X3SS-10 | X3SS-11 | X3SS-12 | X3SS-15 | X3SS-16 | X3SS-17 | X3SS-18 | X3SS-19 | X3SS-29 | X3SS-30 | X3SS-23 | X3SS-24 | X3SS-25 | X3SS-26 |
|---|---|---|---|---|---|---|---|---|---|---|---|---|---|---|---|---|---|---|---|---|
| | Granodiorite | | | | | Diorite enclave | | | | Albitophyre | | | | | K-feldspar granite | | Monzonitic granite | | | |
| $SiO_2$ | 69.9 | 71.4 | 72.5 | 70.3 | 71.2 | 53.8 | 55.4 | 58.8 | 55.6 | 72.0 | 76.4 | 71.7 | 71.3 | 71.2 | 76.5 | 76.7 | 74.0 | 73.8 | 73.5 | 72.9 |
| $TiO_2$ | 0.27 | 0.33 | 0.31 | 0.29 | 0.31 | 0.64 | 0.87 | 0.62 | 0.87 | 0.38 | 0.19 | 0.42 | 0.45 | 0.43 | 0.08 | 0.08 | 0.21 | 0.21 | 0.20 | 0.20 |
| $Al_2O_3$ | 14.5 | 13.2 | 13.0 | 14.5 | 12.8 | 15.6 | 16.4 | 15.1 | 16.1 | 14.9 | 13.5 | 14.1 | 13.9 | 15.2 | 12.5 | 12.4 | 13.6 | 13.3 | 13.4 | 13.2 |
| $Fe_2O_3^T$ | 2.72 | 3.31 | 2.74 | 2.85 | 3.11 | 9.18 | 9.55 | 8.49 | 9.41 | 0.22 | 0.11 | 0.46 | 0.81 | 0.65 | 1.02 | 0.98 | 2.08 | 2.14 | 2.13 | 2.10 |
| MnO | 0.12 | 0.15 | 0.09 | 0.09 | 0.13 | 0.39 | 0.29 | 0.22 | 0.36 | 0.02 | 0.01 | 0.04 | 0.06 | 0.03 | 0.03 | 0.03 | 0.05 | 0.05 | 0.05 | 0.05 |
| MgO | 0.84 | 1.01 | 0.91 | 0.89 | 0.98 | 3.03 | 3.52 | 2.86 | 3.51 | 0.69 | 0.38 | 2.32 | 2.58 | 1.34 | 0.02 | 0.01 | 0.55 | 0.57 | 0.53 | 0.52 |
| CaO | 2.37 | 2.11 | 1.91 | 2.36 | 2.28 | 6.18 | 5.43 | 5.35 | 5.19 | 2.44 | 2.65 | 3.34 | 3.52 | 3.13 | 0.48 | 0.47 | 1.95 | 2.04 | 1.97 | 2.13 |
| $Na_2O$ | 4.21 | 3.69 | 4.14 | 3.94 | 4.22 | 3.66 | 4.12 | 4.28 | 4.70 | 7.80 | 5.74 | 5.86 | 5.60 | 6.49 | 4.05 | 4.03 | 3.55 | 3.87 | 4.17 | 4.03 |
| $K_2O$ | 2.77 | 2.41 | 2.28 | 2.56 | 2.23 | 1.43 | 1.54 | 1.75 | 1.75 | 0.40 | 0.17 | 0.45 | 0.45 | 0.61 | 4.48 | 4.41 | 3.27 | 3.23 | 3.37 | 3.41 |
| $P_2O_5$ | 0.06 | 0.06 | 0.06 | 0.05 | 0.06 | 0.07 | 0.15 | 0.08 | 0.14 | 0.12 | 0.03 | 0.08 | 0.09 | 0.15 | 0.00 | 0.00 | 0.05 | 0.05 | 0.05 | 0.05 |
| LOI | 1.94 | 1.73 | 1.92 | 1.83 | 2.43 | 5.54 | 2.17 | 1.98 | 2.17 | 0.54 | 0.36 | 0.64 | 0.69 | 0.57 | 0.35 | 0.38 | 0.31 | 0.36 | 0.40 | 0.74 |
| Total | 99.6 | 99.4 | 99.8 | 99.6 | 99.7 | 99.5 | 99.5 | 99.5 | 99.8 | 99.6 | 99.5 | 99.4 | 99.5 | 99.7 | 99.6 | 99.5 | 99.6 | 99.6 | 99.7 | 99.4 |
| Mg# | 38 | 38 | 40 | 38 | 38 | 39 | 42 | 40 | 43 | 86 | 87 | 91 | 86 | 80 | 3 | 2 | 34 | 34 | 33 | 33 |
| ACNK | 1.02 | 1.05 | 1.02 | 1.07 | 0.94 | 0.83 | 0.90 | 0.81 | 0.84 | 0.84 | 0.93 | 0.87 | 0.87 | 0.89 | 1.01 | 1.01 | 1.05 | 0.98 | 0.95 | 0.93 |
| ANK | 1.46 | 1.52 | 1.40 | 1.56 | 1.36 | 2.06 | 1.95 | 1.69 | 1.67 | 1.13 | 1.40 | 1.39 | 1.44 | 1.34 | 1.09 | 1.08 | 1.45 | 1.35 | 1.27 | 1.28 |
| Sc | 8.41 | 9.95 | 7.80 | 8.32 | 8.98 | 33.2 | 25.2 | 29.3 | 25.2 | 11.0 | 5.00 | 15.2 | 13.2 | 14.0 | 6.39 | 5.46 | 6.19 | 6.60 | 6.34 | 6.56 |
| V | 39.9 | 48.2 | 36.1 | 43.6 | 41.1 | 238 | 226 | 224 | 222 | 39.8 | 25.1 | 78.7 | 80.9 | 49.7 | 5.74 | 3.30 | 23.8 | 23.6 | 26.1 | 23.4 |
| Cr | 3.46 | 3.41 | 3.41 | 5.92 | 4.07 | 5.04 | 3.63 | 5.12 | 4.91 | 3.39 | 2.58 | 3.77 | 5.04 | 4.57 | 2.19 | 2.01 | 4.86 | 4.61 | 4.99 | 5.11 |
| Co | 4.92 | 5.97 | 5.08 | 5.45 | 5.97 | 20.3 | 19.3 | 20.3 | 20.6 | 0.65 | 0.33 | 6.24 | 0.90 | 1.18 | 0.38 | 0.31 | 3.31 | 3.12 | 3.29 | 3.54 |
| Ni | 1.84 | 1.63 | 1.52 | 2.28 | 2.22 | 4.72 | 3.04 | 3.84 | 3.97 | 1.75 | 0.82 | 6.66 | 2.90 | 3.24 | 0.50 | 0.46 | 2.76 | 2.66 | 2.65 | 2.91 |
| Cu | 5.99 | 14.0 | 2.99 | 4.28 | 12.9 | 164 | 207 | 81.7 | 181 | 3.23 | 1.90 | 25.1 | 3.93 | 3.72 | 1.70 | 1.50 | 2.90 | 2.44 | 3.21 | 3.11 |
| Zn | 78.7 | 93.0 | 71.3 | 64.4 | 110 | 263 | 143 | 157 | 292 | 19.6 | 13.6 | 26.7 | 35.7 | 22.9 | 37.7 | 39.2 | 45.3 | 43.1 | 40.9 | 39.3 |
| Ga | 13.7 | 13.0 | 10.8 | 13.5 | 12.0 | 16.2 | 18.6 | 16.0 | 17.7 | 14.8 | 13.4 | 13.3 | 13.8 | 15.1 | 18.7 | 18.3 | 15.0 | 15.1 | 15.3 | 15.2 |
| Ge | 1.33 | 1.52 | 1.18 | 1.33 | 1.35 | 2.73 | 2.73 | 2.44 | 2.54 | 0.84 | 1.02 | 1.12 | 1.20 | 1.21 | 1.89 | 1.57 | 1.62 | 1.62 | 1.66 | 1.63 |
| Rb | 103 | 93.8 | 80.4 | 90.4 | 76.3 | 73.2 | 69.8 | 62.4 | 76.3 | 10.7 | 4.50 | 18.0 | 17.9 | 20.4 | 221 | 224 | 121 | 118 | 120 | 136 |
| Sr | 228 | 202 | 166 | 191 | 149 | 264 | 231 | 234 | 272 | 180 | 223 | 263 | 250 | 267 | 3.87 | 2.71 | 143 | 143 | 153 | 156 |
| Y | 13.4 | 15.5 | 12.7 | 11.8 | 13.7 | 25.0 | 34.8 | 19.9 | 26.5 | 22.5 | 16.7 | 19.1 | 19.4 | 25.0 | 81.8 | 71.0 | 28.4 | 31.2 | 28.4 | 40.6 |
| Zr | 83.6 | 112 | 78.3 | 91.6 | 92.2 | 46.8 | 76.4 | 81.9 | 83.7 | 120 | 92.8 | 107 | 93.3 | 120 | 99.2 | 93.6 | 133 | 137 | 146 | 142 |
| Nb | 5.33 | 6.25 | 5.44 | 5.57 | 6.11 | 4.28 | 8.00 | 4.52 | 5.86 | 8.03 | 6.74 | 5.70 | 6.13 | 8.49 | 14.4 | 15.8 | 8.20 | 8.05 | 7.60 | 9.49 |
| Cs | 2.09 | 2.07 | 1.74 | 2.07 | 1.63 | 1.93 | 1.62 | 1.30 | 1.53 | 0.27 | 0.27 | 0.50 | 0.62 | 0.43 | 5.59 | 5.10 | 6.70 | 6.45 | 6.25 | 6.70 |
| Ba | 670 | 561 | 431 | 480 | 426 | 308 | 507 | 345 | 556 | 55.4 | 61.6 | 119 | 116 | 75.1 | 24.0 | 8.93 | 472 | 439 | 421 | 424 |
| La | 13.5 | 15.5 | 13.4 | 12.4 | 15.1 | 11.9 | 15.6 | 14.6 | 15.0 | 11.2 | 20.6 | 7.31 | 6.84 | 7.53 | 18.0 | 13.0 | 21.4 | 27.4 | 30.1 | 29.8 |
| Ce | 24.4 | 28.9 | 24.4 | 22.4 | 27.8 | 25.4 | 39.4 | 28.9 | 33.8 | 23.5 | 38.8 | 18.8 | 17.3 | 20.8 | 47.6 | 36.1 | 43.8 | 55.2 | 60.0 | 59.7 |
| Pr | 2.77 | 3.33 | 2.76 | 2.38 | 3.03 | 3.22 | 5.47 | 3.27 | 4.30 | 2.88 | 4.09 | 2.89 | 2.62 | 3.38 | 7.03 | 5.34 | 5.28 | 6.61 | 6.99 | 7.15 |
| Nd | 9.93 | 12.0 | 9.92 | 8.41 | 10.7 | 12.6 | 22.8 | 11.9 | 17.1 | 11.4 | 13.5 | 12.9 | 11.6 | 15.3 | 30.1 | 23.8 | 19.7 | 24.5 | 25.8 | 26.9 |
| Sm | 1.98 | 2.36 | 1.91 | 1.81 | 2.21 | 3.09 | 5.22 | 2.71 | 4.06 | 2.96 | 2.29 | 3.26 | 3.01 | 3.95 | 9.92 | 8.26 | 4.53 | 5.23 | 5.32 | 5.89 |
| Eu | 0.62 | 0.56 | 0.50 | 0.61 | 0.59 | 0.99 | 1.10 | 0.99 | 1.11 | 0.64 | 0.46 | 0.74 | 0.73 | 0.90 | 0.11 | 0.09 | 0.72 | 0.74 | 0.72 | 0.70 |
| Gd | 2.13 | 2.50 | 2.05 | 1.87 | 2.22 | 3.32 | 5.42 | 2.95 | 4.09 | 3.10 | 2.41 | 2.98 | 2.85 | 3.70 | 10.6 | 8.91 | 4.32 | 5.01 | 4.93 | 5.66 |
| Tb | 0.37 | 0.44 | 0.36 | 0.31 | 0.37 | 0.62 | 0.99 | 0.51 | 0.71 | 0.57 | 0.42 | 0.53 | 0.52 | 0.66 | 2.16 | 1.88 | 0.76 | 0.86 | 0.81 | 0.99 |
| Dy | 2.32 | 2.74 | 2.23 | 1.99 | 2.34 | 4.15 | 6.16 | 3.47 | 4.48 | 3.73 | 2.64 | 3.35 | 3.32 | 4.25 | 14.0 | 12.3 | 4.81 | 5.39 | 4.99 | 6.34 |
| Ho | 0.51 | 0.60 | 0.49 | 0.45 | 0.51 | 0.91 | 1.34 | 0.75 | 0.98 | 0.81 | 0.60 | 0.71 | 0.72 | 0.93 | 3.03 | 2.66 | 1.04 | 1.15 | 1.06 | 1.40 |
| Er | 1.51 | 1.79 | 1.45 | 1.34 | 1.52 | 2.74 | 3.94 | 2.21 | 2.88 | 2.42 | 1.83 | 2.11 | 2.10 | 2.68 | 8.82 | 7.88 | 3.05 | 3.36 | 3.09 | 4.15 |
| Tm | 0.24 | 0.28 | 0.23 | 0.21 | 0.24 | 0.43 | 0.62 | 0.34 | 0.44 | 0.37 | 0.30 | 0.32 | 0.33 | 0.42 | 1.31 | 1.19 | 0.46 | 0.51 | 0.46 | 0.66 |
| Yb | 1.64 | 1.94 | 1.56 | 1.48 | 1.66 | 2.99 | 4.21 | 2.29 | 2.98 | 2.49 | 2.05 | 2.40 | 2.39 | 2.86 | 8.76 | 7.77 | 3.12 | 3.42 | 3.13 | 4.47 |
| Lu | 0.27 | 0.32 | 0.25 | 0.25 | 0.28 | 0.49 | 0.67 | 0.37 | 0.48 | 0.39 | 0.33 | 0.43 | 0.44 | 0.47 | 1.33 | 1.18 | 0.49 | 0.54 | 0.50 | 0.73 |
| Hf | 2.80 | 3.37 | 2.62 | 2.82 | 2.75 | 1.53 | 2.62 | 2.53 | 2.37 | 3.54 | 3.31 | 3.32 | 2.80 | 3.54 | 5.02 | 4.71 | 4.22 | 4.39 | 4.73 | 4.79 |
| Ta | 0.58 | 0.66 | 0.58 | 0.59 | 0.65 | 0.34 | 0.64 | 0.46 | 0.40 | 0.61 | 0.81 | 0.53 | 0.51 | 0.68 | 1.58 | 1.65 | 0.79 | 0.81 | 0.73 | 1.03 |
| Pb | 20.6 | 19.8 | 15.8 | 21.4 | 18.4 | 173 | 27.6 | 55.3 | 45.7 | 1.54 | 2.42 | 5.97 | 6.02 | 2.79 | 23.1 | 23.2 | 14.2 | 14.0 | 14.7 | 15.3 |
| Th | 8.99 | 9.87 | 10.19 | 8.11 | 9.75 | 2.60 | 5.11 | 6.59 | 4.04 | 8.21 | 15.3 | 8.18 | 8.78 | 9.79 | 20.1 | 16.4 | 10.8 | 12.5 | 12.1 | 15.0 |
| U | 1.53 | 1.73 | 1.54 | 1.30 | 1.53 | 1.05 | 1.48 | 2.23 | 1.26 | 2.26 | 2.23 | 1.60 | 1.35 | 2.19 | 5.41 | 4.36 | 1.59 | 1.87 | 2.53 | 3.09 |
| $(La/Yb)_N$ | 5.90 | 5.72 | 6.17 | 6.01 | 6.52 | 2.86 | 2.66 | 4.55 | 3.62 | 3.22 | 7.23 | 2.19 | 2.05 | 1.89 | 1.48 | 1.20 | 4.92 | 5.75 | 6.90 | 4.77 |
| $(Gd/Yb)_N$ | 1.07 | 1.06 | 1.09 | 1.04 | 1.10 | 0.92 | 1.07 | 1.07 | 1.14 | 1.03 | 0.97 | 1.03 | 0.99 | 1.07 | 1.00 | 0.95 | 1.15 | 1.21 | 1.30 | 1.05 |
| Eu/Eu* | 0.92 | 0.71 | 0.77 | 1.03 | 0.82 | 0.95 | 0.64 | 1.08 | 0.84 | 0.65 | 0.60 | 0.73 | 0.76 | 0.72 | 0.03 | 0.03 | 0.50 | 0.45 | 0.43 | 0.37 |

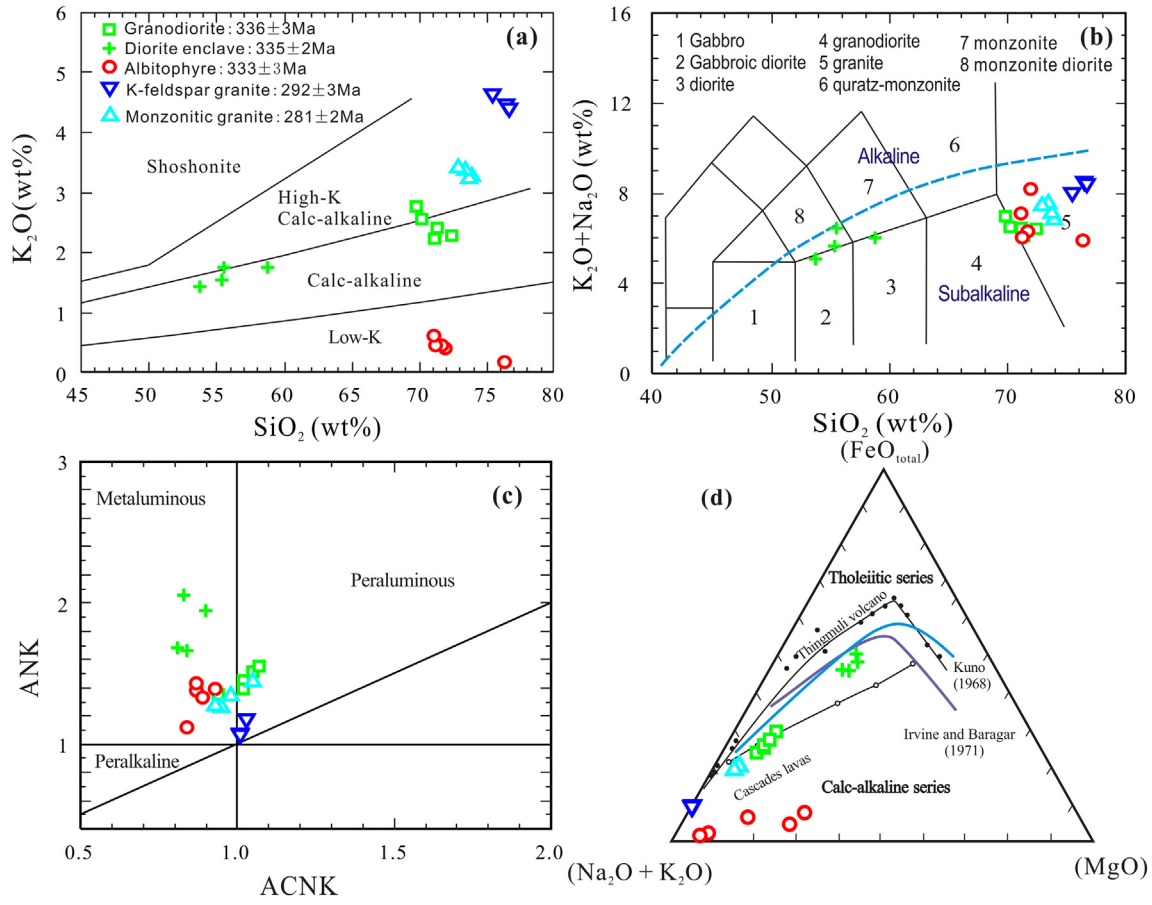


**Fig. 4.** Major element diagrams for the Late Paleozoic felsic plutons. (a) $K_2O$ versus $SiO_2$ diagram (after Irvine and Baragar, 1971); (b) TAS classification diagram (after Middlemost, 1994); (c) ANK versus ACNK diagram (after Maniar and Piccoli, 1989); (d) AFM diagram with boundary between the calc-alkaline and tholeiitic fields (after Irvine and Baragar, 1971).

(4.50–20.4 ppm), Ba (55.4–119 ppm), Cr (2.58–5.04 ppm), Co (0.33–6.24 ppm) and Ni (0.82–6.66 ppm) contents (Table 1). They are characterized by slightly negative Nb, Ta and Ti anomalies, and weakly positive Pb anomalies in a primitive mantle-normalized trace element variation diagram (Fig. 5d). The rocks have similar $\varepsilon_{Nd}(t)$ (−0.69 to −0.37) and $T^2_{DM}$ ages (1135–1161 Ma), but slightly higher initial $^{87}Sr/^{86}Sr$ ratios (0.7065 to 0.7067) than the granodioritic pluton (Table 2).

*5.2.4. K-feldspar granite*

Sample from this pluton have high $SiO_2$ (76.5–76.3 wt.%) and $K_2O$ (4.41–4.48 wt.%), but display low $Fe_2O_3^T$ (0.98–1.02 wt.%) and MgO (0.01–0.02 wt.%), and thus have high $K_2O/Na_2O$ ratios (1.09–1.11). They show high-K calc-alkaline characteristics (Fig. 4a, d and Table 1). These rocks are weakly peraluminous with ASI values 1.01 (Fig. 4c and Table 1) and show slightly LREE-enriched ($(La/Yb)_N = 1.20–1.48$) with flat HREE patterns ($(Ga/Yb)_N = 0.95–1.00$) and remarkably negative Eu anomalies ($Eu/Eu^* = 0.03$) (Fig. 5e). They have high Rb (221–224 ppm), Ga (18.3–18.7 ppm) and Pb (23.1–23.2 ppm), but low Sr (2.71–3.87 ppm) and Ba (8.93–24.0 ppm), thus with high Rb/Sr (57.1–82.8), Rb/Ba (9.21–25.12) and Ga/Al (2.80–2.81) ratios (Table 1). In a primitive mantle normalized diagram, they display strong negative Ba, Nb, Ta, Sr and Ti anomalies, and show positive Rb and Pb anomalies (Fig. 5f). These rocks have much higher $\varepsilon_{Nd}(t)$ (+2.77 to +3.21) and more juvenile $T^2_{DM}$ ages (799–841 Ma) than the granodioritic pluton (Table 2).

*5.2.5. Monzonitic granite*

The monzonitic granite samples also have high $SiO_2$ (73.0–74.0 wt.%) and $K_2O$ (3.23–3.41 wt.%), low $Fe_2O_3^T$ (2.08–2.14 wt.%) and MgO (0.52–0.57 wt.%), with relatively low $K_2O/Na_2O$ ratios (0.81–0.92). These rocks show high-K calc-alkaline characteristics (Fig. 4a, d and Table 1) and are weakly metaluminous to weakly peraluminous ($ASI = 0.93–1.05$) (Fig. 4c and Table 1). In the Chondrite-normalized diagram, they have uniform REE patterns and are characterized by weak LREE enrichment ($(La/Yb)_N = 4.77–6.90$), with relatively flat HREE patterns ($(Ga/Yb)_N = 1.05–1.30$) but strongly negative Eu anomalies ($Eu/Eu^* = 0.37–0.50$) (Fig. 5e and Table 1). The rocks are characterized by remarkably negative anomalies of Ba, Sr, Nb, Ta and Ti anomalies, and positive Rb and Pb anomalies (Fig. 5f). They have homogeneous initial Sr isotope compositions ($(^{87}Sr/^{86}Sr)_i = 0.7042–0.7050$) and positive $\varepsilon_{Nd}(t)$ values (+2.22 to +2.34) similar to those of the granitic pluton, with juvenile $T^2_{DM}$ ages (868–878 Ma).

## 6. Discussion

### 6.1. Petrogenesis and magma source

*6.1.1. Granodiorite and dioritic enclave*

Mafic microgranular enclaves (MMEs) are identified as one of the keys to understand the petrogenesis and evolution of granitoids magma (Donaire et al., 2005; Huang et al., 2014), and have geochemical clues to the entire granitoid-MME system. In general, the MMEs enclosed by granitoids can be formed by four mechanisms, including xenolith captured from the wall-rock, restite separation (Chappell et al., 1987; Chappell and White, 1992; White et al., 1999), cognate cumulate (Donaire et al., 2005; Huang et al., 2014) and magma mixing (Chen et al., 2014; Gou and Zhang, 2016; Guan et al., 2014; Y.Y. Zhang et al., 2015). Zircon U–Pb dating suggests the granodiorites were coeval to the dioritic enclaves (Fig. 3a, b and Supplemental Table S1).

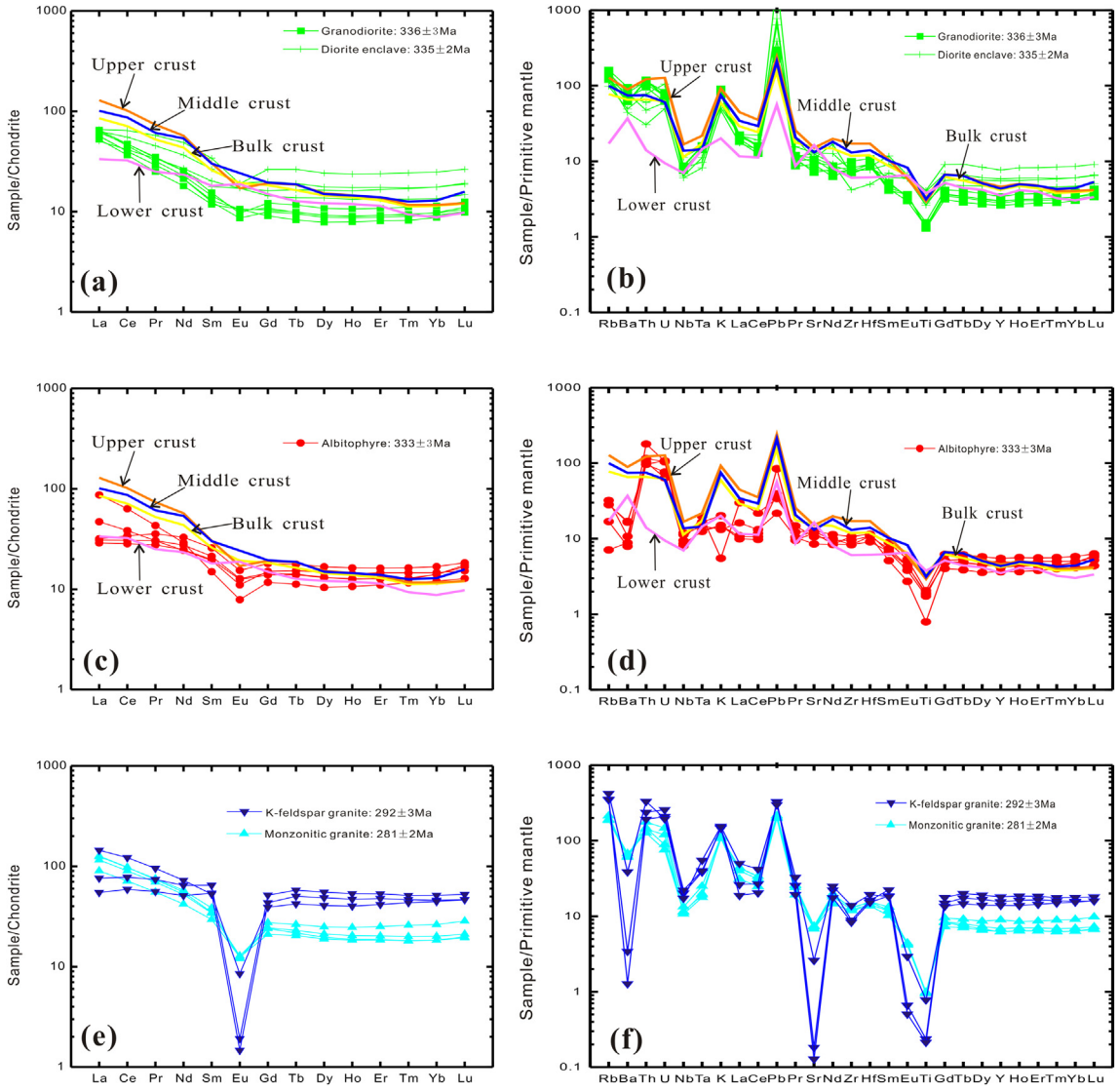


**Fig. 5.** Chondrite-normalized REE patterns (a, c and e) and Primitive mantle-normalized trace element spider diagrams (b, d and f). The data of Chondrite and Primative Mantle are from Sun and McDonough (1989), the data of Upper Crust, Middle Crust, Lower Crust and Bulk Crust are from Rudnick and Gao (2003).

Moreover, the dioritic enclaves show hypidiomorphic granular texture (Fig. 2e, f), thus xenolith captured from the wall-rock and restite separation model can be precluded (Chappell et al., 1987; Chappell and White, 1992; Donaire et al., 2005; Huang et al., 2014). The MMEs have whole-rock Sr–Nd isotopic compositions and zircon U–Pb ages similar to those of the host granodiorites (Fig. 6a, b and Table 2). This may

**Table 2**
Sr–Nd isotopic compositions of the Late Paleozoic felsic plutons.

| Sample | Age (Ma) | Rb (ppm) | Sr (ppm) | $^{87}Rb/^{86}Sr$ | $^{87}Sr/^{86}Sr$ | $2\sigma_m$ | $(^{87}Sr/^{86}Sr)_i$ | Sm (ppm) | Nd (ppm) | $^{147}Sm/^{144}Nd$ | $^{143}Nd/^{144}Nd$ | $2\sigma_m$ | $T^1_{DM}$ (Ma) | $T^2_{DM}$ (Ma) | $\varepsilon_{Nd}(t)$ |
|---|---|---|---|---|---|---|---|---|---|---|---|---|---|---|---|
| X3SS-2 | 336 | 103 | 228 | 1.3095 | 0.711345 | 7 | 0.7051 | 1.98 | 9.93 | 0.1206 | 0.512416 | 19 | 1203 | 1195 | −1.06 |
| X3SS-4 | 336 | 80.4 | 166 | 1.4067 | 0.711733 | 7 | 0.7050 | 1.91 | 9.92 | 0.1167 | 0.512453 | 7 | 1097 | 1121 | −0.17 |
| X3SS-6 | 336 | 76.3 | 149 | 1.4790 | 0.712318 | 7 | 0.7052 | 2.21 | 10.7 | 0.1250 | 0.512478 | 5 | 1158 | 1111 | −0.05 |
| X3SS-9 | 335 | 73.2 | 264 | 0.8032 | 0.709737 | 8 | 0.7059 | 3.09 | 12.6 | 0.1482 | 0.512530 | 6 | 1445 | 1108 | −0.02 |
| X3SS-11 | 335 | 62.4 | 234 | 0.7706 | 0.709243 | 6 | 0.7056 | 2.71 | 11.9 | 0.1383 | 0.512512 | 8 | 1294 | 1104 | 0.03 |
| X3SS-15 | 333 | 10.7 | 180 | 0.1729 | 0.707561 | 8 | 0.7067 | 2.96 | 11.4 | 0.1575 | 0.512523 | 6 | 1700 | 1151 | −0.57 |
| X3SS-17 | 333 | 18.0 | 263 | 0.1985 | 0.707418 | 7 | 0.7065 | 3.26 | 12.9 | 0.1533 | 0.512508 | 10 | 1620 | 1161 | −0.69 |
| X3SS-19 | 333 | 20.4 | 267 | 0.2208 | 0.707547 | 9 | 0.7065 | 3.95 | 15.3 | 0.1556 | 0.512529 | 5 | 1630 | 1135 | −0.37 |
| BLS[a,b] | 318 | 67.2 | 420 | 0.4519 | 0.706209 | 9 | 0.7042 | 6.79 | 28.7 | 0.1491 | 0.512822 | 13 | 778 | 628 | 5.50 |
| BL-065[c] | 318 | 25.6 | 347 | 0.2106 | 0.705710 | 8 | 0.7048 | 1.54 | 7.0 | 0.1330 | 0.512705 | 5 | 840 | 768 | 3.89 |
| BL-058[c] | 314 | 75.1 | 257 | 0.8343 | 0.707630 | 7 | 0.7039 | 2.61 | 10.6 | 0.1488 | 0.512836 | 5 | 740 | 608 | 5.78 |
| BL-050[c] | 307 | 99.4 | 212 | 1.3386 | 0.709820 | 7 | 0.7040 | 2.83 | 11.8 | 0.1450 | 0.512838 | 5 | 690 | 590 | 5.94 |
| X3SS29 | 292 | 221 | 3.87 | 165.50 | 1.467007 | 19 | 0.7792 | 9.92 | 30.1 | 0.1990 | 0.512784 | 5 | 3784 | 841 | 2.77 |
| X3SS30 | 292 | 224 | 2.71 | 239.80 | 1.585897 | 62 | 0.5896 | 8.26 | 23.8 | 0.2095 | 0.512830 | 5 | 11,629 | 799 | 3.27 |
| X3SS24 | 281 | 118 | 143 | 2.3858 | 0.713710 | 9 | 0.7042 | 5.23 | 24.5 | 0.1290 | 0.512627 | 9 | 944 | 878 | 2.22 |
| X3SS26 | 281 | 136 | 156 | 2.5215 | 0.715051 | 7 | 0.7050 | 5.89 | 26.9 | 0.1324 | 0.512640 | 4 | 960 | 868 | 2.34 |

Data sources: a, Zhou et al., 2010; b, Zhang et al., 2013; c, W.F. Zhang et al., 2016.

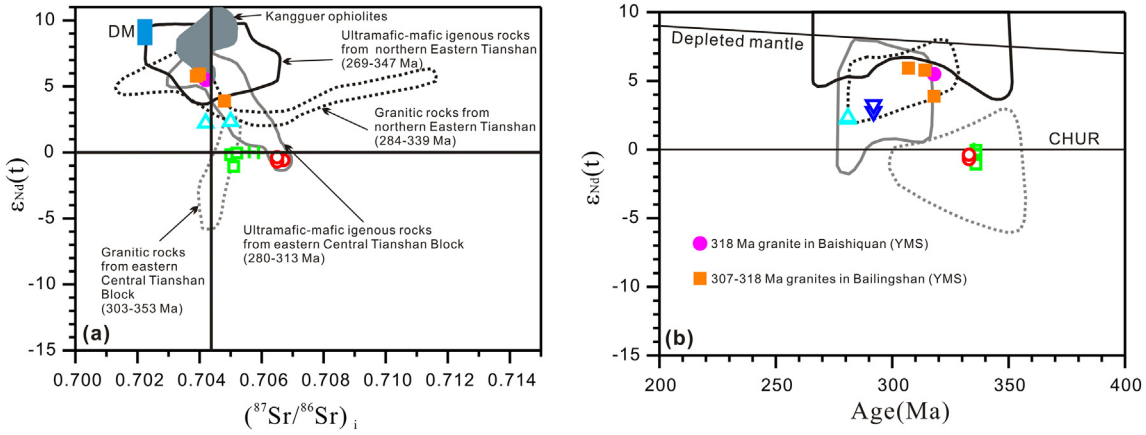


**Fig. 6.** (a) $\varepsilon_{Nd}(t)$ vs. $(^{87}Sr/^{86}Sr)_i$ diagram of the Late Paleozoic felsic plutons from Eastern Tianshan. DM-Depleted mantle. The field of DM is after Zindler and Hart (1986). The data of Kangguer ophiolites are from Li et al. (2008). The data of granitic rocks and ultramafic-mafic igneous rocks from the northern Eastern Tianshan and the eastern Central Tianshan Block are detailed in the Supplemental Table S2. (b) $\varepsilon_{Nd}(t)$ vs. Age (Ma) diagram of the Late Paleozoic felsic plutons from Eastern Tianshan. YMS, the Aqishan-Yamansu belt. Data of the YMS are from Zhou et al. (2010), Zhang et al. (2013), W.F. Zhang et al. (2016) and this study. Symbols same as Fig. 4.

imply a magma mixing of mantle- and crust-derived magmas or cognate cumulate processes (Dahlquist, 2002; Donaire et al., 2005; Huang et al., 2014). However, the MMEs are mineralogically same as their hosts but only differ in modal abundances (Fig. 2d, e, f), which argue for the MMEs and their hosts were formed from the same source (Dahlquist, 2002; Donaire et al., 2005; Huang et al., 2014). Besides, in Th/La vs. Zr/Sm plot, the granodiorites and dioritic enclaves do not support the magma mixing process (Fig. 7a). Collectively, we conclude that the granodiorites and dioritic enclaves were formed by cumulate mechanism. Although cumulate is a common process in the granitoid-MME system, we do not intend to exclude a minor affect from participation of other processes in the evolution of this system. Moreover, as proposed by Donaire et al. (2005), the increase of cumulate process suggests that the magma ascents or emplaces at shallow levels in the crust, but are not relevant to petrogenetic processes at the granite source.

Both the granodiorites and dioritic enclaves have low $Mg^{\#}$ (38–40 and 39–43, respecively), and trace elements similar to the middle and upper crust (Fig. 5a and b; Rudnick and Gao, 2003). They have lower $\varepsilon_{Nd}(t)$ values (−1.06 to −0.05 and −0.02 to 0.03) than contemporaneously mantle-derived mafic rocks (+6.22 to +7.34) (Luo et al., 2012, 2016). Furthermore, they have old two stage Nd model ages (1111–1195 Ma and 1104–1108 Ma) (Table 2), implying that an origin from newly underplated mafic rocks in the lower crust can be ruled out. The granitoids-MME system was most likely derived from the partial melts of Mesoproterozoic crust, which was considered as the Precambrian basement of the Central Tianshan Block (Figs. 6 and 10a). For instance, the depositional time of Xingxingxia group metasedimentary rocks from Weiya, Kumishi and south to the Dikar in the range of 1.2–1.3 Ga, and show $\varepsilon_{Nd}(t)$ values varying from −4.0 to +6.4) (Li et al., 2003). The granitic gneisses from Weiya-Xingxingxia, Pargangtag and Ganggou-Kumishi metamorphic blocks were generated at 1.1–1.2 Ga and have similar $\varepsilon_{Nd}(t)$ values (−5.0 to +5.8) (Liu et al., 2004). Hence, according to Huang et al. (2015, 2017), the eastern Central Tianshan Block has undergone a crustal growth at about 1.4 Ga and the basement rocks show positive $\varepsilon_{Hf}(t)$ values (+0.6 to +10.2). Therefore, we suggest that the Mesoproterozoic basement of the eastern Central Tianshan Block is most likely to be the magma source of the granitoid-MME system.

### 6.1.2. Albitophyre

The albitophyres exhibit high $SiO_2$, low MgO, Cr, Co and Ni contents, combined with Nb/Ta (11.4), Y/Ho (27.3) and Zr/Hf (32.2) ratios (Table 1) similar to those of the bulk continental crust (11.4, 25 and 35.7, respectively; Rudnick and Gao, 2003), reflecting a crustal origin. Moreover, these rocks have near-zero $\varepsilon_{Nd}(t)$ values (−0.69 to −0.37) (Fig. 6 and Table 2) similar to the contemporaneously crust-derived granitoid-MME system. This implies a similar crustal magma source for both types of rocks. Furthermore, the albitophyre samples define a straightly positive correlation line in the La vs. La/Sm diagram

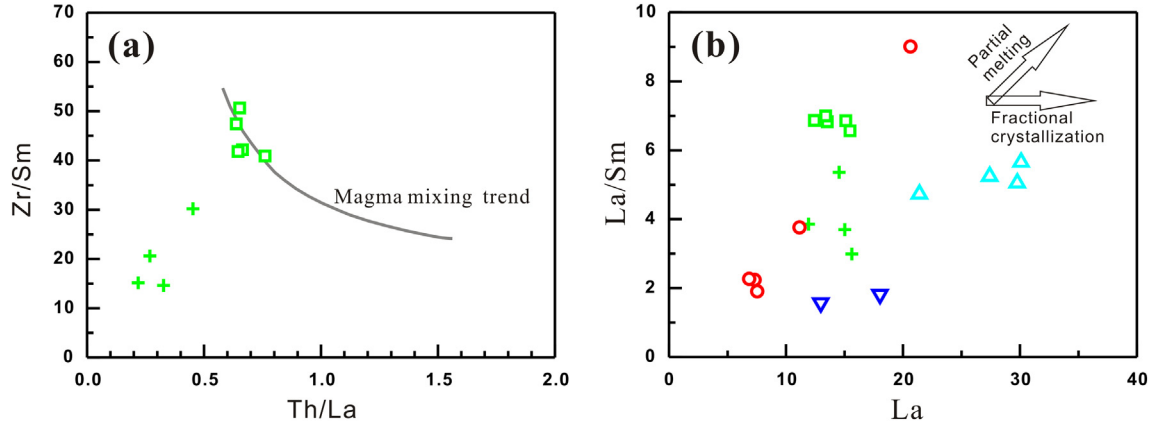


**Fig. 7.** (a) Zr/Sm vs. Th/La diagrams for the Early Carboniferous felsic plutons. (b) La/Sm vs. La diagrams of the Late Paleozoic felsic plutons. Symbols same as Fig. 4.

(Fig. 7b), indicating that their compositional variations are mainly controlled by partial melting. Therefore, we suggest the albitophyres are probably to be products of dehydration melting in the middle and lower crust level, where the significantly low porosity of metamorphic rocks prevents large amounts of water from being involves (Skjerlie et al., 1993; Yuan et al., 2007). However, these rocks have high $Na_2O$ (5.60–7.80 wt.%), low $K_2O$ (0.17–0.61 wt.%) and thus very high $Na_2O/K_2O$ ratios (10.6–34.6) (Table 1). Combined with the corrosion boundary between albite and quartz in the studied samples (Fig. 2g), we suggest that the albitophyres probably experienced a metasomatism of sodic-rich fluids (Li et al., 1999; Tang et al., 2006) during the dehydration melting process.

Compositional diversity of crust-derived melts strongly depends on source compositions and melting conditions (Beard and Lofgren, 1991; Rapp et al., 1991; Yuan et al., 2007; Y.Y. Zhang et al., 2015), thus the chemical and isotopic compositions of igneous rocks can provide much useful information for the petrogenesis. The albitophyres have low to intermediate $Al_2O_3$ (<15.2 wt.%) and Sr (<267 ppm) contents and negative Eu anomalies ($Eu/Eu^* = 0.60–0.76$) (Table 1), which can be ascribed to a plagioclase residuum in the source. Amphibole and mica are the most common hydrous minerals involved in dehydration-melting that generates granitic magmas. For the albitophyre samples in this study, the lack of upwardly-concave, chondrite-normalized REE patterns may suggest that the amphibole was not a major residual phase, consistent with an amphibole dehydration melting reaction (Borg and Clynne, 1998). They have relatively low K, Rb and Cs contents and significant low $K_2O/Na_2O$ (<0.1) and Rb/Sr (<0.1) ratios (Table 1), which argue against mica in their source. These rocks have high $CaO/Na_2O$ (>0.3), $CaO/(MgO + FeO^T)$ and low $Al_2O_3/(MgO + FeO^T)$ ratios (Fig. 8 and Table 1), further suggest that they were formed mainly by dehydration melting of metamorphosed mafic to intermediate rocks which contains abundant amphibole rather than mica-rich pelites and greywackes (Gerdes et al., 2002; Jung and Pfänder, 2007; Yuan et al., 2007).

#### 6.1.3. K-feldspar granite and monzonitic granite

Granitic rocks can be genetically divided into I-, S-, M-, and A-types according to their source rocks and chemical compositions (Bonin, 2007). In general, A-type granites have higher $K_2O + Na_2O$, Fe/Mg, Ga/Al, HFSE (e.g., Zr and Hf) and lower CaO, Sr, Eu and Ba than I- and S-type granites (Bonin, 2007; Collins et al., 1982; King et al., 1997; Whalen et al., 1987). In the $K_2O + Na_2O$ vs. 10,000 Ga/Al and Zr vs. 10,000 Ga/Al diagrams (Fig. 9a, b; Whalen et al., 1987), the K-feldspar granite samples are plotted in the A-type field, where the monzonitic granites plot in the I-, S-, and M-type field. The significantly high HFSE, HREE and FeO/MgO ratios (54.4–98.7), and remarkably low Ba, Sr and Eu contents of the ca. 292 Ma K-feldspar granites (Table 1) suggest that they are A-type granites (Bonin, 2007; Eby, 1992; Pearce et al., 1984; Whalen et al., 1987). The monzonitic granites are metaluminous to weakly peraluminous with A/CNK values ranging from 0.93 to 1.05, and have very low $P_2O_5$ (Fig. 4c and Table 1) in contrast to S-type granites which generally are strongly peraluminous with A/CNK > 1.1 and have high in $P_2O_5$ (Clemens, 2003; Zhao et al., 2008). This signature suggests that ca. 281 Ma monzonitic granites belong to I-type granites, which is also supported by the presence of amphibole instead of cordierite and garnet.

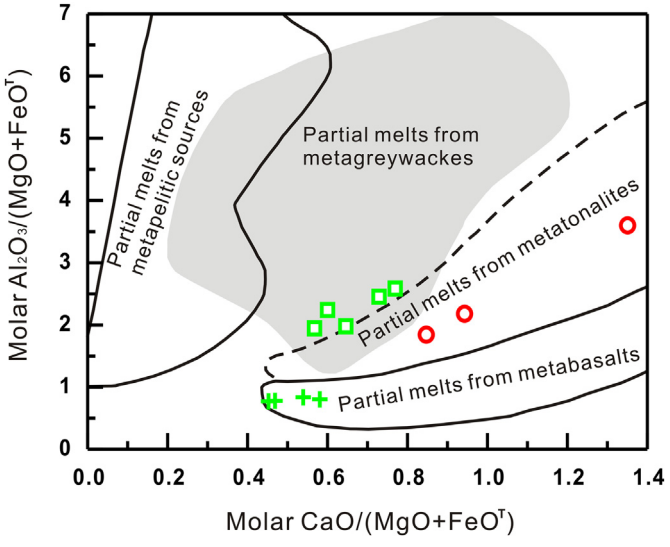


**Fig. 8.** Molar $Al_2O_3/(MgO + FeO^T)$ vs. molar $CaO/(MgO + FeO^T)$ diagram for the Early Carboniferous felsic plutons. Symbols same as Fig. 4.

The petrogenesis and source of A-type granites has long been a debated issue. Several models have been proposed, including strong fractionation of mantle derived magma (Turner et al., 1992), partial melting of various crustal sources (Collins et al., 1982; Eby, 1990; Whalen et al., 1987), or mixing between mantle-derived magma and crustal melt (Yang et al., 2006a). The major concerns of these models focuses on the source regions and the role of the mantle (Wu et al., 2002; Yuan et al., 2010). The high $SiO_2$ (>76%) and low MgO (<0.1%) contents of this A-type granites also preclude a derivation directly from the mantle (Zhao et al., 2008). Moreover, very small proportion of contemporary mafic rocks in the study area indicates they cannot be differentiation products of mantle-derived magmas (Huang et al., 2008). In contrast to La contents, the La/Sm ratios in the K-feldspar granite samples almost remain the same, suggesting various degrees of fractional crystallization (Fig. 7b). The presence of Sr, Eu and Ba negative anomalies in the A-type granites (Fig. 5e-f) are hence indicative of fractionation of both plagioclase and K-feldspar (Huang et al., 2008; Wu et al., 2002). These rocks have relatively flat HREE patterns, which suggests the garnet was absent in the magma source and argues for magma generation under a pressure of 0.8–1.0 Gpa (Patiño Douce and Beard, 1995; Watkins et al., 2007). The positive $\varepsilon_{Nd}(t)$ (+2.77 to +3.21) values preclude a source from highly evolved upper continental crust. The young whole-rock two stage Nd model ages (799–841 Ma) indicate a relatively young crustal source, although a mantle contribution cannot be completely precluded.

Calc-alkaline to high-K calc-alkaline I-type granitoids can be generated by (1) partial melting of mafic to intermediate (meta)-igneous rocks without sediments involved (Chappell and White, 2001; W.F. Zhang et al., 2016) or (2) mingling of juvenile crustal-derived and mantle-derived magmas (Kemp et al., 2007). The ca. 281 Ma monzonitic granites have high $SiO_2$ (>72%) and low MgO (<0.6%), Ba, Sr and Eu contents, but not as remarkable as the K-feldspar granites (Fig. 5e-f and Table 1). The positive $\varepsilon_{Nd}(t)$ values (+2.22 to +2.34), with relatively young $T^2_{DM}$ ages (868–878 Ma) (Table 2), suggesting the monzonitic pluton was also derived from a relatively young crustal source.

### 6.2. Contribution of mantle (juvenile) materials

#### 6.2.1. Early Carboniferous

Whether the Precambrian basement exists in the Aqishan-Yamansu belt or not has long been debated (Luo et al., 2016; Ma et al., 1993). Zhang et al. (1998) reported a specific age of the Precambrian single zircon from a quartz syenite porphyry in the Aqishan-Yamansu belt and suggest a possible Precambrian basement exists underneath this island arc. According to Luo et al. (2016), the age spectra of inherited zircons from the Early Carboniferous volcanic rocks in the Aqishan-Yamansu belt show almost the same peaking ages in their Precambrian records to those recorded from the Central Tianshan Block, which suggest this belt was likely a part of the Central Tianshan Block in the Early Carboniferous. In this study, all the Early Carboniferous granitoids had old $T^2_{DM}$ ages (1104–1195 Ma) and were produced by partial melting of the Mesoproterozoic crust of the eastern Central Tianshan Block, which argue for the Aqishan-Yamansu arc system was closely connected with

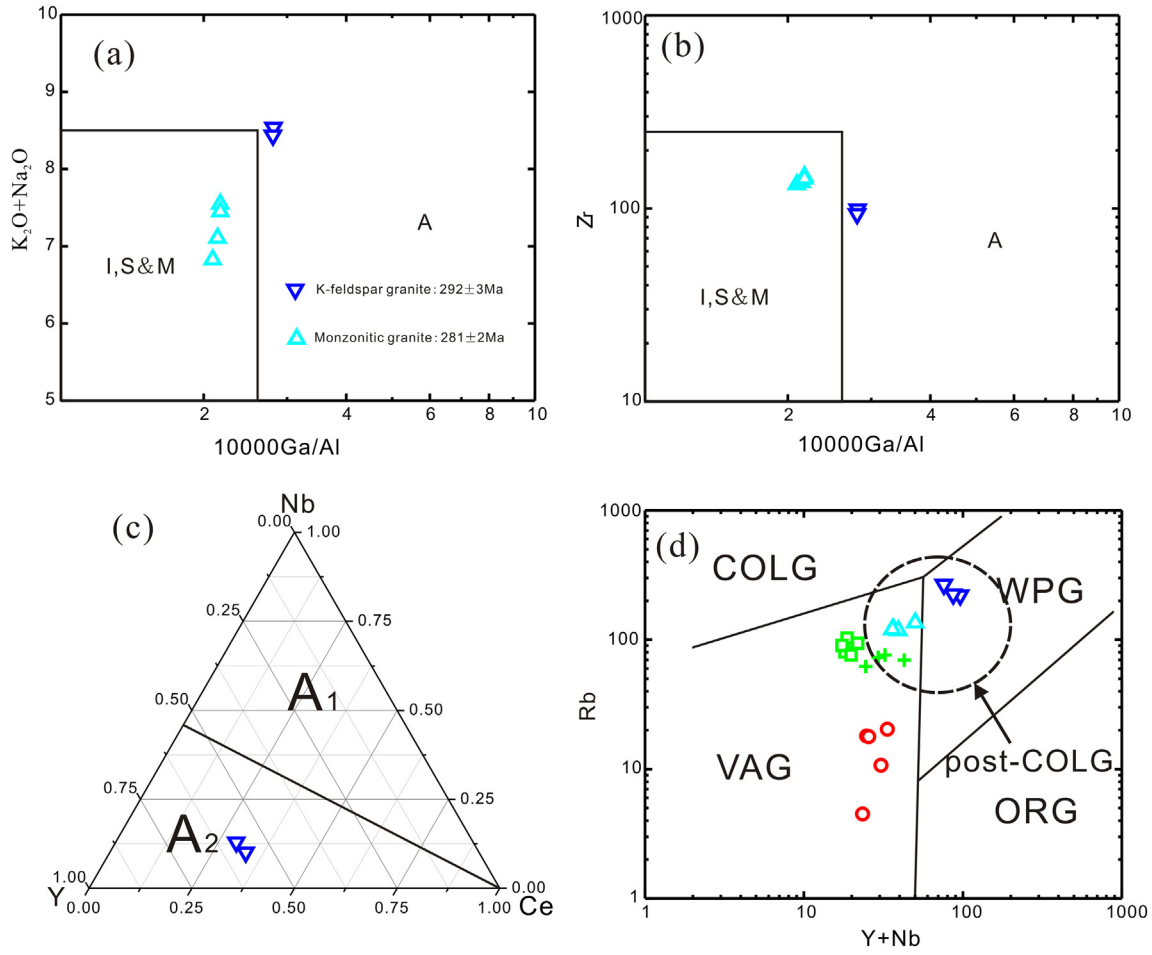


**Fig. 9.** (a) $K_2O + Na_2O$ vs. 10000Ga/Al, (b) Zr vs. 10000Ga/Al, (c) Y–Ce–Nb, (d) Rb vs. Y + Nb diagram for the Late Paleozoic felsic plutons (after Pearce et al., 1984; Whalen et al., 1987). Abbreviations: COLG, collision granite; VAG, volcanic arc granite; ORG, ocean ridge granite; WPG, within plate granite; post-COLG, post collision granite. Symbols same as Fig. 4.

the Central Tianshan Block in the Early Carboniferous. This suggestion is reinforced by their similar Sr–Nd isotopic ratios to the contemporaneous granitic rocks in the eastern Central Tianshan Block (Fig. 6a, b; Supplemental Table S2). Considering similar trace element and Sr–Nd isotopic compositions to the Permian lithospheric mantle-derived ultramafic-mafic rocks (Fig. 6a, b; Supplemental Table S2), mantle component is suggested to input the magma source of the Early Carboniferous granitic plutons. Moreover, the initial crust materials was suggested occurred as old as the late Paleoproterozoic (ca. 1.8 Ga) in the eastern Central Tianshan Block, whereas the Archean basement was absent (Fig. 10a; Hu et al., 2000; Li et al., 2003; Liu et al., 2004 and Huang et al., 2015, 2017). After the Paleoproterozoic crustal growth, the basement of Eastern Tianshan was formed at Mesoproterozoic (ca. 1.2 to 1.4 Ga) with young signatures and young crustal model ages (Hu et al., 2000; Huang et al., 2017). Hence, a simple mixing model using different end-members is show in Fig. 10b. The depleted juvenile endmember is presented by mantle-derived basaltic rocks with chemical compositional within the range of the Kangguer ophiolites (Fig. 6; Jahn et al., 2000c; Li et al., 2008). The old endmember

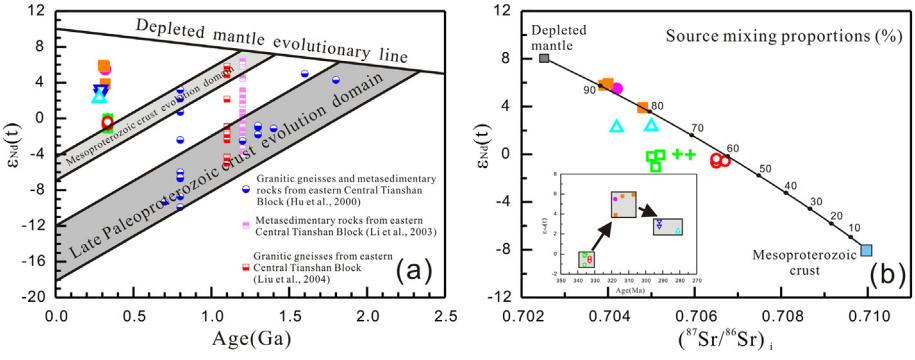


**Fig. 10.** (a) $\varepsilon_{Nd}(t)$ vs. Age (Ga) diagram of the Late Paleozoic felsic plutons from the Aqishan-Yamansu belt and the Paleo- to Mesoproterozoic crust evolution of eastern Central Tianshan Block. (b) $\varepsilon_{Nd}(t)$ vs. $(^{87}Sr/^{86}Sr)_i$ diagram showing source mixing proportions between two end-members. Depleted mantle (represent juvenile components): Sr = 150 ppm, $(^{87}Sr/^{86}Sr)_i = 0.7025$, Nd = 15 ppm, $\varepsilon_{Nd}(t) = +8$ (from Jahn et al., 2000c). Mesoproterozoic crust basement: Sr = 300 ppm, $(^{87}Sr/^{86}Sr)_i = 0.710$, Nd = 24 ppm, $\varepsilon_{Nd}(t) = -8$ (from Rudnick and Fountain, 1995, Hu et al., 2000, Li et al., 2003, Liu et al., 2004). Symbols same as Fig. 6.

is presented by Mesoproterozoic crustal basement rocks containing some late Paleoproterozoic crust materials (Fig. 10b; Rudnick and Fountain, 1995, Hu et al., 2000, Li et al., 2003, Liu et al., 2004). For the Early Carboniferous granitic rocks, the depleted juvenile components added to the magma source are probably 60% (Fig. 10b). Considering the Carboniferous magmatism has a slightly higher $\varepsilon_{Nd}(t)$ values to the Mesoproterozoic crust evolution domain (Fig. 10a), the high mantle contributions were most likely caused by the input of depleted mantle materials into the basement rocks.

#### 6.2.2. Late Carboniferous

Recent zircon U–Pb dating of granodiorites in the Bailinshan area yielded late Carboniferous ages at ca. 318 Ma (Zhou et al., 2010). These rocks has positive $\varepsilon_{Nd}(t)$ values (+5.50) and juvenile $T^2_{DM}$ ages (~628 Ma) (Figs. 6a, b, 10a, b; Table 2; Zhang et al., 2013). Lately, three other Late Carboniferous granitic plutons (318 Ma, 314 Ma and 307 Ma, respectively) were also reported in the Bailinshan area (W.F. Zhang et al., 2016). The granitic rocks also have positive $\varepsilon_{Nd}(t)$ values (Mean + 3.89, +5.78 and +5.94, respectively) and juvenile two stage Nd model ages averagely at 768 Ma, 608 Ma and 590 Ma, respectively) (Figs. 6a, b, 10a, b and Table 2). These Late Carboniferous rocks were thought to be derived from the partial melts of a mixed source involving dominantly basaltic lower crust and minor mature crust-derived materials (W.F. Zhang et al., 2016). Near the Bailinshan area, the ca. 310 Ma basalts and tuffs have positive $\varepsilon_{Nd}(t)$ values (+2.8 to +7.1), which were considered to be sourced from a depleted lithosphere mantle (garnet-bearing peridotite) (Zhang et al., 2013). These lower crust-derived granitic plutons and depleted mantle-derive basic volcanic rocks in the Aqishan-Yamansu belt have similar $\varepsilon_{Nd}(t)$ values and all of them are plotted within the range of the igneous rocks in the northern Eastern Tianshan (Fig. 6; Supplemental Table S2). On account of the ultramafic-mafic rocks with the same Sr–Nd isotopic ratios to the depleted mantle (Fig. 6; Zindler and Hart, 1986), no Precambrian basement exists in the northern Eastern Tianshan. Therefore, the juvenile Nd model ages of these Late Carboniferous rocks suggest that more depleted mantle materials were added into the crust than those in the Early Carboniferous, which indicate a crustal transition from old basement to juvenile crust in the Aqishan-Yamansu belt. This conclusion was evidenced by the two end-member mixing calculation of the magma source (Fig. 10b), in which about 80% to 90% juvenile components were added into the Late Carboniferious granitic magma sources.

#### 6.2.3. Early Permian

The two Early Permian granitic plutons have $\varepsilon_{Nd}(t)$ values (+2.22 to +3.27) higher and $T^2_{DM}$ ages (799–878 Ma) younger than the Early Carboniferous plutons in both the Aqishan-Yamansu belt and the eastern Central Tianshan Block (Table 2; Figs. 6; 10a, b; Supplemental Table S2), suggesting that more depleted components were added to the crustal source during this time. However, the slight decrease of the $\varepsilon_{Nd}(t)$ values with increasing $T^2_{DM}$ ages than those of the Late Carboniferous samples indicate that different juvenile components were likely added to the magma source in different tectonic settings. Although the juvenile materials are as high as ~75% for the Early Permian rocks, their old lower crust components are slightly increased from the Late Carboniferous to the Early Permian (Fig. 10b). Because the Sr–Nd isotopic ratios of the Early Permian rocks in the Aqishan-Yamansu belt are similar to those of both the coeval ultramafic-mafic rocks in the eastern Central Tianshan Block and the coeval granitic rocks in the northern Eastern Tianshan (Fig. 6a, b), it is suggested that the Aqishan-Yamansu belt and adjacent terranes had formed an united continental crust prior to the Early Permian and were then extensively underplated by mantle-derived magmas during the Early Permian.

### 6.3. Implications for tectonic evolution

#### 6.3.1. Early Carboniferous

Although the tectonic evolution of the Aqishan-Yamansu belt has been widely discussed (Hou et al., 2014; Luo et al., 2012, 2016; Xiao et al., 2004, 2013; W.F. Zhang et al., 2016), its tectonic setting in Late Paleozoic is still controversial. Xiao et al. (2004) suggested the Aqishan-Yamansu belt was a Devonian to Early Permian island arc formed by north-dipping subduction of the South Tianshan oceanic plate. Whereas the south-dipping subduction of the paleo-Tianshan oceanic plate was suggested to generate the Yamansu-Central Tianshan continental margin arc (Hou et al., 2014; Luo et al., 2016). However, other hypothesises suggested that the Aqishan-Yamansu in the south and the Dananhu island arc in the north was produced by the bipolar subduction of the Kangguer oceanic lithosphere (Hou et al., 2006; Y.H. Wang et al., 2014).

In this study, the Early Carboniferous granodiorites and dioritic enclaves in the Aqishan-Yamansu belt have Nb, Ta and Ti depletion and LILE (Rb and Ba) enrichment, showing geochemical features similar to subduction-related magmatic rocks (Mcculloch and Gamble, 1991). This interpretation is supported by the plotting of these samples into the arc-related field in the Rb vs. Y + Nb discrimination diagram (Pearce et al., 1984; Whalen et al., 1987) (Fig. 9d). Moreover, their remarkable depleted juvenile components added to a magma source also argue for the arc-related tectonic seeting. Besides, the arc-related tectonic setting is consistent with the results of some recent studies. For instance, a calc-alkaline volcanic rocks series in the Yamansu group yielded coeval zircon U–Pb ages of 348 ± 2, 336 ± 2 and 334 ± 3 Ma (Luo et al., 2012, 2016). Zircon U–Pb dating of the Xifengshan and Shiyingtan granites and Changtiaoshan quartz diorite porphyrite yielded similar Early Carboniferous ages of 349 ± 3 Ma, 342 ± 11 Ma and 338 ± 3 Ma, respectively (Zhou et al., 2010). A granodiorite in the Hongyuntan area also has an Early Carboniferous age of 329 ± 9 Ma (Wu et al., 2006) (Fig. 1b). Therefore, a magmatic arc was likely built on the Aqishan-Yamansu belt along the northern margin of the Central Tianshan Block in the Early Carboniferous (at least from 349 to 329 Ma).

However, there is still controversial regarding to the formation of the Aqishan-Yamansu arc and the subduction polarity with which oceanic lithosphere was responsible for the generation of this arc system. According to the Sm–Nd isochron dating of the eclogites (ca. 347 Ma) and $^{40}Ar/^{39}Ar$ plateau ages (ca. 334 and 331 Ma) of phengite from an omphacite-phengite-bearing blueschist (Gao and Klemd, 2003), which formed in a Paleozoic accretionary wedge on the southern side of the Yili-Central Tianshan block, Gao and Klemd (2003) suggested the subduction of the South Tianshan Ocean plate may have been completely finished by the end of the Early Carboniferous (W.F. Zhang et al., 2016). Besides, the Early Permian (273–283 Ma) granitic plutons in Kokshalboth area of South Tianshan Mountains simultaneously occurred in the Yili-Central Tianshan blocks in the north and the Tarim Craton in the south. As typical stitching plutons, Early Permian granitic plutons suggested the west South Tianshan ocean was closed before 300 Ma (Liu et al., 2013). Moreover, the closure of the South Tianshan Orogenic Belt was considered as a scissor-type in which the east part was closed earlier than the west part (Gao et al., 2009). Furthermore, new zircon U–Pb ages (ca. 320 Ma) for the South Tianshan eclogites indicate that collision between the Tarim Craton and the Yili-Central Tianshan blocks occurred during the Late Carboniferous (Su et al., 2010). Therefore, the Aqishan-Yamansu arc was unlikely related to the subduction of the South Tianshan oceanic lithosphere below the eastern Central Tianshan Block. Instead, the southwards subduction of the Kangguer (Northern Tianshan) oceanic lithosphere was more likely responsible for the formation of the continental marginal arc.

As suggested by the similar age spectra of inherited zircons in the Early Carboniferous volcanic rocks to those of the Central Tianshan basement (Luo et al., 2012, 2016), the Early Carboniferous granitic plutons were considered to be produced by partial melting of ancient

continental crust, indicating the Aqishan-Yamansu belt was possibly developed on the northern margin of the Central Tianshan Block. This model is further supported by: (1) Ophiolites with prolonged ages (494 to 330 Ma) along the Kangguer fault representing remnants of the Kangguer ocean plate (Li et al., 2008; Liu et al., 2016). (2) The ca. 330 Ma MORB-type basalt from the Wutongwozi Formation in the Kangguer belt (Li et al., 2008; Supplemental Table S2). (3) The existence of 338–347 Ma arc-related granitic plutons along the Kangguer belt (B. Wang et al., 2014), as well as the 320–325 Ma arc-related granitic gneisses on the northern margin of the Central Tianshan Block (X.R. Zhang et al., 2015). (4) The Early Carboniferous Yamansu Formation in the northern Aqishan-Yamansu belt and the Late Carboniferous Tugutublak Formation in the southern (Muhetaer et al., 2014; W.F. Zhang et al., 2016), consistent with typical subduction processes along continental margin arcs (W.F. Zhang et al., 2016).

*6.3.2. Late Carboniferous*

Some Late Carboniferous calc-alkaline granitic intrusions in the Bailinshan area yielded zircon U–Pb ages of 307 to 318 Ma. They have similar major and trace element contents, but with significantly elevated $\varepsilon_{Nd}(t)$ values and younger Nd model ages related to the Early Carboniferous granitic plutons (Zhang et al., 2013; W.F. Zhang et al., 2016; Zhou et al., 2010) (Fig. 6 and Table 2). These rocks were suggest to be produced by partial melting of a juvenile lower crust that was mixed with mantle-derived material in a back (intra)-arc extension basin (W.F. Zhang et al., 2016) and more than 80% juvenile components proportions were added to the crust. The Late Carboniferous back (intra)-arc extension tectonic setting is also evidenced by the ca. 320 Ma MORB-like volcanic rocks from the Tugutubulake and Wutongwozi Formations, which are geochemically similar to those of the back-arc basin basalt from the Mariana and Okinawa troughs (Luo et al., 2016). Therefore, there is a tectonic transition from Early Carboniferous continental margin arc to Late Carboniferous back (intra)-arc extension setting in the studied area. Besides, as discussed in the previous sections, southwards subduction of the Kangguer (Northern Tianshan) oceanic lithosphere below the eastern Central Tianshan Block was responsible for the Early Carboniferous continental marginal arc. Therefore, the regional extension was probably associated with the roll-back of the Kangguer oceanic lithosphere which formed the Late Carboniferous Aqishan-Yamansu intra-arc basin. Indeed, we favor the hypothesis that the Aqishan-Yamansu belt in the south and the Dananhu island arc in the north were produced by the bipolar subduction of the Kangguer oceanic lithosphere (Hou et al., 2006; Y.H. Wang et al., 2014).

*6.3.3. Early Permian*

Although the Early Permian volcanic rocks and granitic plutons were sparsely in the Aqishan-Yamansu belt (Wang et al., 2005; Zhou et al., 2010) (Fig. 1b), they were widely exposed in neighboring regions. For instance, B. Wang et al. (2014) reported ca. 275 Ma gabbro and diorite in the East Huangshan and Kangguertag areas and ca. 290 Ma granitic plutons in the East Huangshan area. X.R. Zhang et al. (2016) reported some ca. 290 Ma mafic-intermediate intrusions from the northern Central Tianshan Block. Some K-feldspar granitic plutons along the Central Tianshan Block have yielded zircon U–Pb ages of 300 ± 3 to 263 ± 2 Ma (Dong et al., 2011; Ma et al., 2015). The large distributions of Early Permian igneous rocks in the Kangguer belt and the Central Tianshan Block show typical geochemical features of post-collisional magmatism in extensional settings, which indicate the Kangguer Ocean was closed before Early Permian (Dong et al., 2011; Ma et al., 2015; B. Wang et al., 2014; X.R. Zhang et al., 2016). Comparatively, the ca. 292 Ma $A_2$-type K-feldspar granitic rocks in this study also support an extension environment and all of our Early Permian samples dominantly plot into the post-collisional field in the Rb vs. Y + Nb discrimination diagrams (Pearce et al., 1984; Whalen et al., 1987) (Fig. 9c, d). Because the widely mantle-derived magma underplating were generally accompanied by a post-collisional extension setting (e.g., Ma et al., 2015; Yuan et al., 2010), the notably juvenile components added to the magma source (~75%) of the studied Early Permian rocks suggest that a post-collisional environment was suitable in the Early Permian. Such a tectonic setting is also evidenced by the newly paleomagnetic and structural studies: (a) a systemic paleomagnetic research, in which, Wang et al. (2007) noted that there were no significant relative motions among the Tarim, Yili and Junggar terranes since the Late Carboniferous; (b) structural analyses showed Eastern Tianshan were a dominance of post-collisional transcurrent shearing in the post-Carboniferous sedimentary and volcanic rocks instead of subduction-/collision-related metamorphism (B. Wang et al., 2014). Therefore, the Early Permian Aqishan-Yamansu granitic plutons were most likely emplaced in a post-collisional extension setting.

## 7. Conclusions

1. The Early Carboniferous granodioritic pluton and the dioritic enclaves were derived from partial melts of the Mesoproterozoic basement of the eastern Central Tianshan Block. The coeval albitophyric pluton was formed by dehydration melting of metamorphosed mafic to intermediate rocks.
2. The Early Permian K-feldspar granitic and monzonitic granitic plutons were derived from a relatively young crustal source.
3. From the Early Carboniferous to Early Permian, the mantle contribution of the felsic magmatic rocks in the Aqishan-Yamansu belt changes from ~60% to ~75%.
4. The remarkably increasing of mantle materials in the magma source was most likely induced by the tectonic transition from an Early Carboniferous continental arc to an Early Permian post-collisional extension environment.

Supplementary data to this article can be found online at https://doi.org/10.1016/j.lithos.2018.02.010.

## Acknowledgements

We thank the Editor and the two reviewers for their constructive comments that have greatly improved the manuscript. This study was supported by National Basic Research Program of China (2014CB440801) and National Natural Science Foundation of China (41522202 and 41603028).

## References

Beard, J.S., Lofgren, G.E., 1991. Dehydration melting and watersaturated melting of basaltic and andesitic greenstones and amphibolites at 1, 3 and 6.9 kb. Journal of Petrology 32, 365–401.

BGMRXUAR (Bureau of Geology and Mineral Resources of Xinjiang Uygur Autonomous Region), 1993. Regional Geology of Xinjiang Uygur Autonomous Region. Geological Publishing House, pp. 1–841 (in Chinese).

Bonin, B., 2007. A-type granites and related rocks: evolution of a concept, problems and prospects. Lithos 97, 1–29.

Bonin, B.L., Azzouni-Sekkal, A., Bussy, F., Ferrag, S., 1998. Alkali-calcic and alkaline post-orogenic (PO) granite magmatism: petrologic constraints and geodynamic setting. Lithos 45, 45–70.

Borg, L.E., Clynne, M.A., 1998. The petrogenesis of felsic calcalkaline magmas from the southernmost Cascades, California: origin by partial melting of basaltic lower crust. Journal of Petrology 39, 1197–1222.

Chappell, B.W., White, A.J.R., 1992. I-Type and S-Type Granites in the Lachlan Fold Belt. Transactions of the Royal Society of Edinburgh: Earth Sciences 83, 1–26.

Chappell, B.W., White, A.J.R., 2001. Two contrasting granite types: 25 years later. Australian Journal of Earth Sciences 48, 489–499.

Chappell, B.W., White, A.J.R., Wyborn, D., 1987. The importance of residual source material (restite) in granite petrogenesis. Journal of Petrology 28, 1111–1138.

Charvet, J., Shu, L.S., Laurent-Charvet, S., 2007. Paleozoic structural and geodynamic evolution of eastern Tianshan (NW China): welding of the Tarim and Junggar plates. Episodes 30, 162–186.

Charvet, J., Shu, L.S., Laurent-Charvet, S., Wang, B., Faure, M., Cluzel, D., Chen, Y., Jong, K.D., 2011. Palaeozoic tectonic evolution of the Tianshan belt, NW China. Science China Earth Sciences 54, 166–184.

Chen, Y.J., Pirajno, F., Wu, G., Qi, J.P., Xiong, X.L., 2012. Epithermal deposits in North Xinjiang, NW China. International Journal of Earth Sciences 101, 889–917.

Chen, Y.X., Song, S.G., Niu, Y.L., Wei, C.J., 2014. Melting of continental crust during subduction initiation: A case study from the Chaidanuo peraluminous granite in the North Qilian suture zone. Geochimica et Cosmochimica Acta 132, 311–336.
Clemens, J.D., 2003. S-type granitic magmas–petrogenetic issues, models and evidence. Earth-Science Reviews 61, 1–18.
Collins, W.J., Beams, S.D., White, A.J.R., Chappell, B.W., 1982. Nature and origin of A-type granites with particular reference to southeastern Australia. Contributions to Mineralogy and Petrology 80, 189–200.
Dahlquist, J.A., 2002. Mafic microgranular enclaves: early segregation from metaluminous magma (Sierra de Chepes), Pampean Ranges, NW Argentina. Journal of South American Earth Sciences 15, 643–655.
Donaire, T., Pascual, E., Pin, C., Duthou, J.L., 2005. Microgranular enclaves as evidence of rapid cooling in granitoid rocks: the case of the Los Pedroches granodiorite, Iberian Massif, Spain. Contributions to Mineralogy and Petrology 149, 247–265.
Dong, Y.P., Zhang, G.W., Neubauer, F., Liu, X.M., Hauzenberger, C., Zhou, D.W., Li, W., 2011. Syn- and post-collisional granitoids in the Central Tianshan orogen: geochemistry, geochronology and implications for tectonic evoution. Gondwana Research 20, 568–581.
Du, L., Long, X.P., Yuan, C., Zhang, Y.Y., Huang, Z.Y., Sun, M., Zhao, G.C., Xiao, W.J., 2018. Early Paleozoic dioritic and granitic plutons in the Eastern Tianshan Orogenic Belt, NW China: constraints on the initiation of a magmatic arc in the Southern Central Asian Orogenic Belt. Journal of Asian Earth Sciences 153, 139–153.
Eby, G.N., 1990. The A-type granitoids – a review of their occurrence and chemical characteristics and speculations on their petrogenesis. Lithos 26, 115–134.
Eby, G.N., 1992. Chemical subdivision of the A-type granitoids: petrogenetic and tectonic implications. Geology 20, 641–644.
Fan, C.Z., Hu, M.Y., Zhao, L.H., Sun, D.Y., Zhan, X.C., 2012. Advances in in situ microanalysis of U–Pb zircon geochronology using laser ablation-inductively coupled plasma-mass spectrometry. Rock and Mineral Analysis 31, 29–46 (in Chinese with English abstract).
Frost, B.R., Barnes, C.G., Collins, W.J., Arculus, R.J., Ellis, D.J., Frost, C.D., 2001. A geochemical classification for granitic rocks. Journal of Petrology 42, 2033–2048.
Gao, J., Klemd, R., 2003. Formation of HP–LT rocks and their tectonic implications in the western Tianshan Orogen, NW China: geochemical and age constraints. Lithos 66, 1–22.
Gao, J., Qian, Q., Long, L.L., Zhang, X., Li, J.L., Su, W., 2009. Accretionary orogenic process of Western Tianshan, China. Geological Bulletin of China 28, 1804–1816 (in Chinese with English abstract).
Gao, J., Klemd, R., Qian, Q., Zhang, X., Li, J.L., Jiang, T., Yang, Y.Q., 2011. The collision between the Yili and Tarim blocks of the Southwestern Altaids: geochemical and age constraints of a leucogranite dike crosscutting the HP–LT metamorphic belt in the Chinese Tianshan Orogen. Tectonophysics 499, 118–131.
Gerdes, A., Montero, P., Bea, F., Fershater, G., 2002. Peraluminous granites frequently with mantle-like isotope compositions: the continental-type Murzinka and Dzhabyk batholiths of the eastern Urals. International Journal of Earth Sciences 91, 3–19.
Gou, L.L., Zhang, L.F., 2016. Geochronology and petrogenesis of granitoids and associated mafic enclaves from Xiate in Chinese Southwest Tianshan: implications for early Paleozoic tectonic evolution. Journal of Asian Earth Sciences 115, 40–61.
Griffin, W.L., Powell, W.J., Pearson, N.J., O'Reilly, S.Y., 2008. GLITTER: date reduction software for laser ablation ICP-MS. Mineralogical Association Canada Short Course 40, 308–311.
Guan, Y.L., Yuan, C., Sun, M., Wilde, S., Long, X.P., Huang, X.L., Wang, Q., 2014. I-type granitoids in the eastern Yangtze Block: implications for the Early Paleozoic intracontinental orogeny in South China. Lithos 206–207, 34–51.
Hou, G.S., Tang, H.F., Liu, C.Q., 2006. Geochemical characteristics of the Late Paleozoic Volcanics in Jueluotage tectonic belt, eastern Tianshan and its implications. Acta Petrologica Sinica 22, 1167–1177 (in Chinese with English abstract).
Hou, T., Zhang, Z.C., Santosh, M., Encarnacion, J., Zhu, J., Luo, W.Q., 2014. Geochronology and geochemistry of submarine volcanic rocks in the Yamansu iron deposit, Eastern Tianshan Mountains, NW China: constraints on the metallogenesis. Ore Geology Reviews 56, 487–502.
Hu, A.Q., Zhang, G.X., Zhang, Q.F., Chen, Y.B., 1998. Constraints on the age of basement and crustal growth in Tianshan Orogen by Nd isotopic composition. Science in China Series D-Earth Sciences 41, 648–657.
Hu, A.Q., Jahn, B.M., Zhang, G.X., Chen, Y.B., Zhang, Q.F., 2000. Crustal evolution and Phanerozoic crustal growth in northern Xinjiang: Nd isotopic evidence. Part I. Isotopic characterization of basement rocks. Tectonophysics 328, 15–51.
Huang, X.L., Xu, Y.G., Li, X.H., Li, W.X., Lan, J.B., Zhang, H.H., Liu, Y.S., Wang, Y.B., Li, H.Y., Luo, Z.Y., Yang, Q.J., 2008. Petrogenesis and tectonic implications of Neoproterozoic, highly fractionated A-type granites from Mianning, South China. Precambrian Research 165, 190–204.
Huang, H., Niu, Y.L., Nowell, G., Zhao, Z.D., Yu, X.H., Zhu, D.C., Mo, X.X., Ding, S., 2014. Geochemical constraints on the petrogenesis of granitoids in the East Kunlun Orogenic belt, northern Tibetan Plateau: Implications for continental crust growth through syn-collisional felsic magmatism. Chemical Geology 370, 1–18.
Huang, Z.Y., Long, X.P., Kröner, A., Yuan, C., Wang, Y.J., Chen, B., Zhang, Y.Y., 2015. Neoproterozoic granitic gneisses in the Chinese Central Tianshan Block: implications for tectonic affinity and Precambrian crustal evolution. Precambrian Research 269, 73–89.
Huang, Z.Y., Long, X.P., Wang, X.C., Zhang, Y.Y., Du, L., Yuan, C., Xiao, W.J., 2017. Precambrian evolution of the Chinese Central Tianshan Block: constraints on its tectonic affinity to the Tarim Craton and responses to supercontinental cycles. Precambrian Research 295, 24–37.
Irvine, T.N., Baragar, W.R.A., 1971. A guide to the chemical classification of the common volcanic rocks. Canadian Journal of Earth Sciences 8, 523–548.
Jahn, B.M., Wu, F.Y., Chen, B., 2000a. Granitoids of the Central Asian Orogenic Belt and continental growth in the Phanerozoic. Transactions of the Royal Society of Edinburgh: Earth Sciences 91, 181–193.
Jahn, B.M., Wu, F.Y., Chen, B., 2000b. Massive granitoid generation in Central Asia: Nd isotope evidence and implication for continental growth in the Phanerozoic. Episodes 23, 82–92.
Jahn, B.M., Wu, F.Y., Hong, D.W., 2000c. Important crustal growth in the Phanerozoic: isotopic evidence of granitoids from east-central Asia. Proceedings of the Indian Academy of Sciences–Earth and Planetary Sciences 109, 5–20.
Jahn, B.M., Windley, B., Natal'in, B., Dobretsov, N., 2004. Phanerozoic continental growth in Central Asia. Journal of Asian Earth Sciences 23, 599–603.
Jung, S., Pfänder, J.A., 2007. Source composition and melting temperatures of orogenic granitoids: constraints from $CaO/Na_2O$, $Al_2O_3/TiO_2$ and accessory mineral saturation thermometry. European Journal of Mineralogy 19, 859–870.
Kemp, A.I.S., Hawkesworth, C.J., Foster, G.L., Paterson, B.A., Woodhead, J.D., Hergt, J.M., Gray, C.M., Whitehouse, M.J., 2007. Magmatic and crustal differentiation history of granitic rocks from hafnium and oxygen isotopes in zircon. Science 315, 980–983.
King, P.L., White, A.J.R., Chappell, B.W., Allen, C.M., 1997. Characterization and origin of aluminous A-type granites from the Lachlan Fold Belt, Southeastern Australia. Journal of Petrology 38, 371–391.
Kröner, A., Windley, B.F., Badarch, G., Tomurtogoo, O., Hegner, E., Jahn, B.M., Gruschka, S., Khain, E.V., Wingate, M.T.D., 2007. Accretionary growth and crust formation in the Central Asian Orogenic Belt and comparison with the Arabian–Nubian shield. Geological Society of America Memoirs 200, 181–209.
Li, Y., Su, C.Q., Liu, J.Q., 1999. Characteristics and genesis of the albitite in the east Qinling Orogenic belt. Acta Petrologica et Mineralogica 18, 121–127 (in Chinese with English abstract).
Li, Q.G., Liu, S.W., Han, B.F., Zhang, J., Chu, Z.Y., 2003. Nd isotopic characteristics of Proterozoic metasedimentary rocks and constraints on their provenance in the eastern segment of Central Tianshan Belt, Xinjiang. Progress in Natural Science 13, 908–913.
Li, X.H., Li, Z.X., Wingate, M.T.D., Chung, S.L., Liu, Y., Lin, G.C., Li, W.X., 2006. Geochemistry of the 755 Ma Mundine Well dyke swarm, northwestern Australia: Part of a Neoproterozoic mantle superplume beneath Rodinia? Precambrian Research 146, 1–15.
Li, W.Q., Ma, H.D., Wang, R., Wang, H., Xia, B., 2008. SHRIMP dating and Nd-Sr isotopic tracing of Kanggurtage ophiolite in eastern Tianshan, Xinjiang. Acta Petrologica Sinica 4, 773–780 (in Chinese with English abstract).
Li, W., Chen, J.L., Dong, Y.P., Xu, X.Y., Li, Z.P., Liu, X.M., He, D.F., 2016. Early Paleozoic subduction of the Paleo-Asian Ocean: zircon U–Pb geochronological and geochemical evidence from Kalatag high-Mg andesites, East Tianshan. Acta Petrologica Sinica 32 (2), 505–521 (in Chinese with English abstract).
Liu, Y., Liu, H.C., Li, X.H., 1996. Simultaneous and precise determination of 40 trace elements in rocksamples using ICP-MS. Geochimica 25, 552–558 (in Chinese with English abstract).
Liu, S.W., Guo, Z.J., Zhang, Z.C., Li, Q.G., Zheng, H.F., 2004. Nature of the Precambrian metamorphic blocks in the eastern segment of Central Tianshan: Constraint from geochronology and Nd isotopic geochemistry. Science in China Series D: Earth Sciences 47, 1085–1094.
Liu, B., Chen, Z.L., Ren, R., Han, B.F., Su, L., 2013. Timing of the South Tianshan suture zone: new evidence of zircon ages from the granitic plutons in Kokshal area. Geological Bulletin of China 32, 1371–1384 (in Chinese with English abstract).
Liu, W.G., Zhang, J.D., Zhao, H.L., 2016. Geological Characteristics and geochronology of Dongdagou oceanic crust remmants in Eastern Tianshan, Xinjiang. Western Exploration Engineering 6, 130–133 (in Chinese).
Long, X.P., Yuan, C., Sun, M., Safonova, I., Xiao, W.J., Wang, Y.J., 2012. Geochemistry and U–Pb detrital zircon dating of Paleozoic graywackes in East Junggar, NW China: insights into subduction-accretion processes in the southern Central Asian Orogenic Belt. Gondwana Research 21, 637–653.
Long, X.P., Wilde, S.A., Wang, Q., Yuan, C., Wang, X.C., Li, J., Jiang, Z.Q., Dan, W., 2015. Partial melting of thickened continental crust in central Tibet: evidence from geochemistry and geochronology of Eocene adakitic rhyolites in the northern Qiangtang Terrane. Earth and Planetary Science Letters 414, 30–44.
Long, L.L., Wang, J.B., Wang, Y.W., Mao, Q.G., Deng, X.H., Zhao, L.T., Sun, Z.Y., Sun, Y., Gao, Y.H., 2016. Discussion on the age of ore-host volcanic strata in the Kalatage ore concentration area, eastern Tianshan: evidence from SHRIMP zircon U–Pb dating. Mineral Exploration 7 (1), 31–37 (in Chinese with English abstract).
Ludwig, K.R., 2003. User's Manual for Isoplot 3.00. A Geochronological Toolkit for Microsoft Excel, Berkeley Geochronology Center. Special Publication, No. 4a (Berkeley,CA).
Luo, T., Liao, Q.A., Chen, J.P., Zhang, X.H., Guo, D.B., Hu, Z.C., 2012. LA-ICP-MS zircon U–Pb dating of the volcanic rocks from Yamansu Formation in the Eastern Tianshan, and its geological significance. Earth Science - Journal of China University of Geosciences 6, 1338–1352 (in Chinese with English abstract).
Luo, T., Liao, Q.A., Zhang, X.H., Chen, J.P., Wang, G.C., Huang, X., 2016. Geochronology and geochemistry of Carboniferous metabasalts in eastern Tianshan, Central Asia: evidence of a back-arc basin. International Geology Review 58, 756–772.
Ma, R.S., Wang, C., Ye, S., 1993. The Outline of Plate Tectonics and Crustal Evolution in the Eastern Tianshan Belt, China. Publishing House of Nanjing University, p. 225 (in Chinese with English abstract.).
Ma, X.X., Shu, L.S., Meert, J.G., Li, J.Y., 2014. The Paleozoic evolution of Central Tianshan: geochemical and geochronological evidence. Gondwana Research 25, 797–819.
Ma, X.X., Shu, L.S., Meert, J.G., 2015. Early Permian slab breakoff in the Chinese Tianshan belt inferred from the post-collisional granitoids. Gondwana Research 27, 228–243.
Maniar, P.D., Piccoli, P.M., 1989. Tectonic discrimination of granitoids. Geological Society of America Bulletin 101, 635–643.
Mcculloch, M.T., Gamble, J.A., 1991. Geochemical and geodynamical constraints on subduction zone magmatism. Earth and Planetary Science Letters 102, 358–374.
Middlemost, E.A.K., 1994. Naming materials in the magma igneous rock system. Earth Science Reviews 37, 215–224.

Muhetaer, Z., Nijat, A., Wu, Z., 2014. Geochemical characteristics of volcanics from the Southern Jueluotage Area and their constraints on the tectonic of Paleo-Asian Ocean. Earth Science Frontiers 21, 1–13 (in Chinese with English abstract).
Patiño Douce, A.E., 1999. What do experiments tell us about the relative contributions of crust and mantle to the origin of granitic magmas? In: Carstro, A., Fernandez, C., Vigneresse, J.L. (Eds.), Understanding Granites: Integrating New and Classic Techniques. Geological Society, London, Special Publications 168, pp. 55–75
Patiño Douce, A., Beard, J.S., 1995. Dehydration–melting of biotite and quartz amphibolite from 3 to 15 kb. Journal of Petrology 36, 707–738.
Pearce, J.A., Harris, N.B.W., Tindle, A.G., 1984. Trace element discrimination diagrams for the tectonic interpretation of granitic rocks. Journal of Petrology 25, 956–983.
Qin, K.Z., Sun, S., Li, J.L., Fang, T.H., Wang, S.L., Liu, W., 2002. Paleozoic epithermal Au and Cu deposits in North Xinjiang, China: epochs, features, tectonic linkage and exploration significance. Resource Geology 52, 291–300.
Rapp, R.P., Watson, E.B., 1995. Dehydration of metabasalt at 8–32 kbar: implications for continental growth and crust–mantle recycling. Journal of Petrology 36, 891–931.
Rapp, R.P., Watson, E.B., Miller, C.F., 1991. Partial melting of amphibolite/eclogite and the origin of Archean trondhjemites and tonalites. Precambrian Research 51, 1–25.
Rudnick, R.L., Fountain, D.M., 1995. Nature and composition of the continental crust: a lower crustal perspective. Reviews of Geophysics 33, 267–309.
Rudnick, R.L., Gao, S., 2003. Composition of The Continental Crust. 3. Elsevier-Pergamon, Oxford, pp. 1–64.
SengÖr, A.M.C., Natalin, B.A., 1996. Turkic-type orogeny and its role in the making of the continental crust. Annual Review of Earth and Planetary Sciences 24, 263–337.
SengÖr, A.M.C., Natalin, B.A., Burtman, V.S., 1993. Evolution of the Altaid tectonic collage and Paleozoic crustal growth in Eurasia. Nature 364, 299–307.
Skjerlie, K.P., Patiño Douce, A.E., Johnston, A.D., 1993. Fluid absent melting of a layered crustal protolith — implications for the generation of anatectic granites. Contributions to Mineralogy and Petrology 114, 365–378.
Su, W., Gao, J., Klemd, R., Li, J.L., Zhang, X., Li, X.H., Chen, N.S., Zhang, L., 2010. U–Pb zircon geochronology of Tianshan eclogites in NW China: implication for the collision between the Yili and Tarim blocks of the southwestern Altaids. European Journal of Mineralogy 22, 473–478.
Sun, S.S., McDonough, W.F., 1989. Chemical and isotopic systematics of oceanic basalts: implications for mantle composition and processes. Geological Society, London, Special Publications 42, 313–345.
Tang, J.H., Gu, L.X., Zheng, Y.C., Fang, T.H., Zhang, Z.Z., Gao, J.H., Wang, F.T., Wang, C.S., Zhang, G.H., 2006. Petrology, geochemistry and genesis of the Na-rich volcanic rocks of the Kalatag area, eastern Tianshan. Acta Petrologica Sinica 22, 1150–1166 (in Chinese with English abstract).
Tang, G.J., Chung, S.L., Hawkesworth, C.J., Cawood, P.A., Wang, Q., Wyman, D.A., Xu, Y.G., Zhao, Z.H., 2017. Short episodes of crust generation during protracted accretionary processes: evidence from Central Asian Orogenic Belt, NW China. Earth and Planetary Science Letters 464, 142–154.
Turner, S.P., Foden, J.D., Morrison, R.S., 1992. Derivation of some A-type magmas by fractionation of basaltic magma — an example from the Padthaway Ridge, South Australia. Lithos 28, 151–179.
Wang, L.S., Li, H.Q., Chen, Y.C., Liu, D.Q., 2005. Geological feature andmineralization epoch of Bailingshan iron deposit, Hami, Xingjiang, China. Mineral Deposits 24, 280–284 (in Chinese with English abstract).
Wang, B., Chen, Y., Zhan, S., Shu, L.S., Faure, M., Cluzel, D., Charvet, J., Laurent-Charvet, S., 2007. Primary Carboniferous and Permian paleomagnetic results from the Yili Block (NW China) and their implications on the geodynamic evolution of Chinese Tianshan Belt. Earth and Planetary Science Letters 263, 288–308.
Wang, B., Cluzel, D., Jahn, B.M., Shu, L.S., Chen, Y., Zhai, Y.Z., Branquet, Y., Barbanson, L., Sizaret, S., 2014a. Late Paleozoic pre- and syn-kinematic plutons of the Kangguer-Huangshan Shear zone: inference on the tectonic evolution of the Eastern Chinese North Tianshan. American Journal of Science 314, 43–79.
Wang, Y.H., Xue, C.J., Liu, J.J., Wang, J.P., Yang, J.T., Zhang, F.F., Zhao, Z.N., Zhao, Y.J., Liu, B., 2014b. Early Carboniferous adakitic rocks in the area of the Tuwu deposit, eastern Tianshan, NW China: slab melting and implications for porphyry copper mineralization. Journal of Asian Earth Sciences 103, 1–18.
Watkins, J., Clemens, J., Treloar, P., 2007. Archaean TTGs as sources of younger granitic magmas: melting of sodic metatonalites at 0.6–1.2 GPa. Contributions to Mineralogy and Petrology 154, 91–110.
Whalen, J.B., Currie, K.L., Chappell, B.W., 1987. A-type granites: geochemical characteristics, discrimination and petrogenesis. Contributions to Mineralogy and Petrology 95, 407–419.
White, A.J.R., Chappell, B.W., Wyborn, D., 1999. Application of the restite model to the Deddick granodiorite and its enclaves — a reinterpretation of the observations and data of Maas et al. (1997). Journal of Petrology 40, 413–421.
Windley, B.F., Allen, M.B., Zhang, C., Zhao, Z.Y., Wang, G.R., 1990. Paleozoic accretion and Cenozoic redeformation of the Chinese Tien Shan Range, central Asia. Geology 18, 128.
Windley, B.F., Alexeiev, D., Xiao, W., Kröner, A., Badarch, G., 2007. Tectonic models for accretion of the Central Asian Orogenic Belt. Journal of the Geological Society of London 164, 31–47.
Wu, F.Y., Sun, D.Y., Li, H.M., Jahn, B.M., Wilde, S., 2002. A-type granites in northeastern China: age and geochemical constraints on their petrogenesis. Chemical Geology 287, 143–173.
Wu, C.Z., Zhang, Z.Z., Zaw, K., Della-Pasque, F., Tang, J.H., Zheng, Y.C., Wang, C.S., San, J.Z., 2006. Geochronology, geochemistry and tectonic significances of the Hongyuntan granitoids in the Qoltag area, Eastern Tianshan. Acta Petrologica Sinica 22, 1121–1134 (in Chinese with English abstract).
Wu, F.Y., Li, X.H., Yang, J.H., Zheng, Y.F., 2007. Discussions on the petrogenesis of granites. Acta Petrologica Sinica 23, 1217–1238.
Xiao, W.J., Zhang, L.C., Qin, K.Z., Sun, S., Li, J.L., 2004. Paleozoic accretionary and collisional tectonics of the eastern Tianshan (China): implications for the continental growth of the central Asia. American Journal of Science 304, 370–395.
Xiao, W.J., Han, C.M., Yuan, C., Sun, M., Lin, S.F., Chen, H.L., Li, Z.L., Li, J.L., Sun, S., 2008. Middle Cambrian to Permian subduction-related accretionary orogenesis of Northern Xinjiang, NW China: implications for the tectonic evolution of central Asia. Journal of Asian Earth Sciences 32, 102–117.
Xiao, W.J., Windley, B.F., Allen, M.B., Han, C.M., 2013. Paleozoic multiple accretionary and collisional tectonics of the Chinese Tianshan orogenic collage. Gondwana Research 23, 1316–1341.
Yakubchuk, A., 2004. Architecture and mineral deposit settings of the Altaid orogenic collage: a revised model. Journal of Asian Earth Sciences 23, 761–779.
Yang, J.H., Wu, F.Y., Chung, S.L., Wilde, S.A., Chu, M.F., 2006a. A hybrid origin for the Qianshan A-type granite, northeast China: geochemical and Sr–Nd–Hf isotopic evidence. Lithos 89, 89–106.
Yang, J.H., Wu, F.Y., Shao, J.A., Wilde, S.A., Xie, L.W., Liu, X.M., 2006b. Constraints on the timing of uplift of the Yanshan Fold and Thrust Belt, North China. Earth and Planetary Science Letters 246, 336–352.
Yuan, H.L., Gao, S., Liu, X.M., Li, H.M., Gunther, D., Wu, F.Y., 2004. Accurate U–Pb age and trace element determinations of zircon by laser ablation-inductively coupled plasma-mass spectrometry. Geostandards and Geoanalytical Research 28, 353–370.
Yuan, C., Sun, M., Xiao, W.J., Li, X.H., Chen, H.L., Lin, S.F., Xia, X.P., Long, X.P., 2007. Accretionary orogenesis of the Chinese Altai: insights from Paleozoic granitoids. Chemical Geology 242, 22–39.
Yuan, C., Sun, M., Wilde, S., Xiao, W.J., Xu, Y.G., Long, X.P., Zhao, G.C., 2010. Post-collisional plutons in the Balikun area, East Chinese Tianshan: evolving magmatism in response to extension and slab break-off. Lithos 119, 269–288.
Zhang, L.C., Ji, J.S., Zeng, Z.R., Li, H.Q., 1998. Isotopic chronology and significance of subvolcanics in Kanggur gold district of east Tianshan. Xinjiang Geology 16, 158–162 (in Chinese with English abstract).
Zhang, X.H., Huang, X., Chen, J.P., Liao, Q.A., Duan, X.F., 2012. Stratigraphical sequence of carboniferous marine volcanic-deposit rock and its geological age in Juoluotage area, eastern Tianshan. Earth Science - Journal of China University of Geosciences 6, 1305–1314 (in Chinese with English abstract).
Zhang, D.Y., Zhou, T.F., Yuan, F., Fiorentini, M.L., Said, N., Lu, Y.J., Pirajno, F., 2013. Geochemical and isotopic constraints on the genesis of the Jueluotage native copper mineralized basalt, Eastern Tianshan, Northwest China. Journal of Asian Earth Sciences 73, 317–333.
Zhang, Y.Y., Sun, M., Yuan, C., Xu, Y.G., Long, X.P., Tomurhuu, D., Wang, C.Y., He, B., 2015a. Magma mixing origin for high Ba–Sr granitic pluton in the Bayankhongor area, central Mongolia: response to slab roll-back. Journal of Asian Earth Sciences 113, 353–368.
Zhang, X.R., Zhao, G.C., Eizenhöfer, P.R., Sun, M., Han, Y.G., Hou, W.Z., Liu, D.X., Wang, B., Liu, Q., Xu, B., 2015b. Latest Carboniferous closure of the Junggar Ocean constrained by geochemical and zircon U–Pb–Hf isotopic data of granitic gneisses from the Central Tianshan Block, NW China. Lithos 238, 26–36.
Zhang, W.F., Chen, H.Y., Han, J.S., Zhao, L.D., Huang, J.H., Yang, J.T., Yan, X.L., 2016a. Geochronology and geochemistry of igneous rocks in the Bailingshan area: Implications for the tectonic setting of late Paleozoic magmatism and iron skarn mineralization in the eastern Tianshan, NW China. Gondwana Research 38, 40–59.
Zhang, X.R., Zhao, G.C., EizenhÖfer, P.R., Sun, M., Han, Y.G., Hou, W.Z., Liu, D.X., Wang, B., Liu, Q., Xu, B., Zhu, C.Y., 2016b. Tectonic transition from Late Carboniferous subduction to Early Permian post-collisional extension in the Eastern Tianshan, NW China: Insights from geochronology and geochemistry of mafic-intermediate intrusions. Lithos 256–257, 269–281.
Zhao, X.F., Zhou, M.F., Li, J.W., Wu, F.Y., 2008. Association of Neoproterozoic A- and I-type granites in South China: implications for generation of A-type granites in a subduction-related environment. Chemical Geology 257, 1–15.
Zhou, T.F., Yuan, F., Zhang, D.Y., Fan, Y., Liu, S., Peng, M.X., Zhang, J.D., 2010. Geochronology, tectonic setting and mineralization of granitoids in Jueluotage area, eastern Tianshan, Xinjiang. Acta Petrologica Sinica 26, 478–502 (in Chinese with English abstract).
Zindler, A., Hart, S., 1986. Chemical geodynamics. Annual Review of Earth and Planetary Sciences 14, 493–571.